CellPress

Molecular Cell
Article

Mechanism of Polyubiquitination by Human Anaphase-Promoting Complex: RING Repurposing for Ubiquitin Chain Assembly

Nicholas G. Brown,[1] Edmond R. Watson,[1,2] Florian Weissmann,[3] Marc A. Jarvis,[3] Ryan VanderLinden,[1,4] Christy R.R. Grace,[1] Jeremiah J. Frye,[1] Renping Qiao,[3] Prakash Dube,[5,6] Georg Petzold,[3] Shein Ei Cho,[1] Omar Alsharif,[1] Ju Bao,[1] Iain F. Davidson,[3] Jie J. Zheng,[1] Amanda Nourse,[1] Igor Kurinov,[7] Jan-Michael Peters,[3,*] Holger Stark,[5,6,*] and Brenda A. Schulman[1,4,*]

[1]Department of Structural Biology, St. Jude Children's Research Hospital, Memphis, TN 38105, USA
[2]Department of Microbiology, Immunology and Biochemistry, University of Tennessee Health Sciences Center, Memphis, TN 38163, USA
[3]Research Institute of Molecular Pathology (IMP), 1030 Vienna, Austria
[4]Howard Hughes Medical Institute, St. Jude Children's Research Hospital, Memphis, TN 38105, USA
[5]Max Planck Institute for Biophysical Chemistry, 37077 Göttingen, Germany
[6]Department of 3D Electron Cryomicroscopy, Institute of Microbiology and Genetics, Georg-August Universität, 37077 Göttingen, Germany
[7]NE-CAT, Bldg. 436E, Department of Chemistry and Chemical Biology, Cornell University, Argonne, IL 60439, USA
*Correspondence: jan-michael.peters@imp.ac.at (J.-M.P.), hstark1@gwdg.de (H.S.), brenda.schulman@stjude.org (B.A.S.)
http://dx.doi.org/10.1016/j.molcel.2014.09.009

SUMMARY

Polyubiquitination by E2 and E3 enzymes is a predominant mechanism regulating protein function. Some RING E3s, including anaphase-promoting complex/cyclosome (APC), catalyze polyubiquitination by sequential reactions with two different E2s. An initiating E2 ligates ubiquitin to an E3-bound substrate. Another E2 grows a polyubiquitin chain on the ubiquitin-primed substrate through poorly defined mechanisms. Here we show that human APC's RING domain is repurposed for dual functions in polyubiquitination. The canonical RING surface activates an initiating E2-ubiquitin intermediate for substrate modification. However, APC engages and activates its specialized ubiquitin chain-elongating E2 UBE2S in ways that differ from current paradigms. During chain assembly, a distinct APC11 RING surface helps deliver a substrate-linked ubiquitin to accept another ubiquitin from UBE2S. Our data define mechanisms of APC/UBE2S-mediated polyubiquitination, reveal diverse functions of RING E3s and E2s, and provide a framework for understanding distinctive RING E3 features specifying ubiquitin chain elongation.

INTRODUCTION

Regulating protein function often involves precisely coordinated posttranslational modification by ubiquitin (Ub). First, an E1 enzyme generates a covalent E2∼Ub intermediate, linked by a thioester bond between the catalytic Cys of an E2 enzyme (approximately 30 in humans) and the C terminus of the "donor" Ub to be transferred ("∼" denotes covalent bond, thioester in E2∼Ub, and isopeptide in Ub∼Ub). An E2∼Ub intermediate then functions with an E3 to transfer Ub to a remotely bound protein substrate. The approximately 600 human E3s in the RING family are thought to function by their RING domains binding specific E2∼Ub intermediates through homologous, yet distinctive, E3-E2∼Ub interfaces (Metzger et al., 2014). RING-dependent stabilization of a particular "closed" E2∼Ub conformation has been shown to immobilize the thioester bond to spark reactivity toward a lysine nucleophile (Berndsen et al., 2013; Dou et al., 2012, 2013; Plechanovová et al., 2012; Pruneda et al., 2012; Reverter and Lima, 2005; Saha et al., 2011; Scott et al., 2014; Wickliffe et al., 2011). Targeting specificity depends in part on the E2 active site; some E2s react promiscuously with many lysines, whereas others target particular protein lysines or N termini such as in Ub itself during formation of polyUb chains with specific Ub∼Ub linkages (Mattiroli and Sixma, 2014). Although this canonical mechanism has been implicated in activating over a dozen RING E3-E2∼Ub intermediates, whether any of the hundreds of other RING E3 and E2 enzymes together promote Ub ligation through other means remains unknown.

A particularly vexing question is whether distinct mechanisms can regulate Ub chain formation. Indeed, polyubiquitination, wherein different chain lengths, sites, and linkage types may be generated, plays a major role in determining fates of modified targets. Some RING E3s use a two-step/two-E2 mechanism to catalyze polyubiquitination (Rodrigo-Brenni and Morgan, 2007; Wu et al., 2010a). First, an "initiating" E2 transfers one or a few Ubs to a substrate. Second, a polyUb chain is assembled with a "chain-elongating" E2 dedicated to producing Ub∼Ub (i.e., di-Ub) linkages. This second E2 generally transfers a donor Ub from its catalytic Cys to a specific Lys on a substrate-linked "acceptor" Ub. This mechanism is used by the anaphase-promoting complex/cyclosome (APC) to control passage through mitosis by catalyzing timely polyubiquitination of cell-cycle regulators such as cyclin B (Primorac and Musacchio, 2013).

The 1.2 MDa multisubunit APC can be viewed as structurally comprising two conformationally dynamic and functionally linked superdomains: the RING-containing "Platform" and the

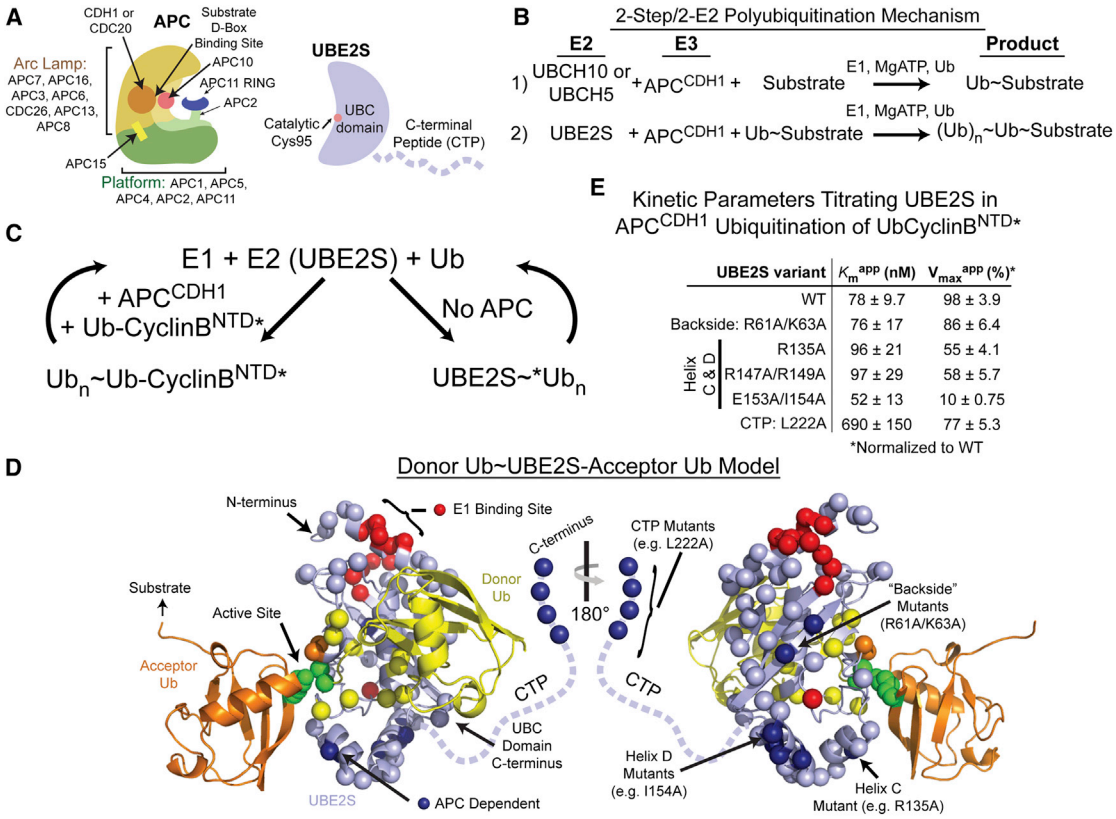

Figure 1. Multiple Atypical E2 Surfaces Dictate UBE2S Binding and Activation by APC

(A) Cartoons of APC and UBE2S highlighting their domains.

(B) Reaction scheme for two-step/two-E2 polyubiquitination by human APC. An "initiating" E2, either UBCH10 or UBCH5, ligates Ub directly to a substrate. The "elongating" E2 UBE2S extends a polyUb chain on the Ub-primed substrate.

(C) Two-part in vitro assay to identify UBE2S surfaces working with APC; (1) 135 UBE2S mutants were tested for APC^{CDH1}-catalyzed polyubiquitination of fluorescent Ub-$CyclinB^{NTD*}$, (2) faulty mutants in part 1 were filtered out for APC-independent defects by assaying UBE2S autoubiquitination.

(D) Results of UBE2S mutant scan depicted on modeled ^{Donor}Ub~UBE2S-^{Acceptor}Ub intermediate, with donor Ub (yellow) from UBCH5~Ub docked on the UBE2S UBC domain (Plechanovová et al., 2012; Sheng et al., 2012) and acceptor Ub (orange) modeled from Wickliffe et al., (2011). UBE2S CTP is represented with a dashed line. Active site; green spheres (UBE2S catalytic Cys, donor Ub G76, acceptor Ub K11). Sites of APC-dependent defects; blue spheres (UBC domain backside and helices C and D, and CTP terminus). Sites of APC-independent defects; red, yellow, and orange spheres for E1, donor Ub, and acceptor Ub-binding sites, respectively. Sites mutated with no defects; slate spheres.

(E) Kinetic parameters from titrating concentration of UBE2S (WT or mutant) in APC^{CDH1}-mediated ubiquitination of Ub-$CyclinB^{NTD*}$ to provide insights into how mutations impaired binding to, and activation by, APC. SEM, $n \geq 3$.

See also Figure S1.

substrate-binding "Arc Lamp" (Figure 1A) (Buschhorn et al., 2011; Chang et al., 2014; Dube et al., 2005; Herzog et al., 2009; Schreiber et al., 2011). In the Platform, APC1, APC4, and APC5 anchor a cullin-RING-like APC2-APC11 catalytic core (Figure 1A). The Arc Lamp provides a substrate-binding site by securing the C termini of APC10 and a coactivator (CDC20 or CDH1), which corecruit substrate motifs such as the "D-box" found in the N-terminal domain (NTD) of cyclin B. APC10 and co-activators also have domains that bind the Platform, and their substrate engagement is thought to propagate conformational changes that enhance APC11 RING domain binding to an initiating E2 that modifies substrate (in humans, typically UBCH10, but also UBCH5 in vitro), and also to the Ub chain-elongating E2 in yeast (Chang et al., 2014; Kimata et al., 2008; Van Voorhis and Morgan, 2014). However, a lingering question is how APC from higher eukaryotes functions with the distinctive chain-elongating E2, UBE2S, to mediate polyubiquitination.

UBE2S has many features differing from E2s that are typically activated by RING E3s. First, the available data imply that UBE2S engages APC in a distinct, but unknown, manner, because the canonical E2 UBCH10 does not compete with UBE2S for binding to APC (Williamson et al., 2009). Second, the UBE2S~Ub intermediate adopts the closed, activated E2~Ub conformation on its own, obviating the need for a RING to stabilize the reactive architecture (Wickliffe et al., 2011). Third, UBE2S's catalytic *ub*iquitin-conjugating (UBC) domain generates free Lys11-linked polyUb chains by substrate-assisted catalysis, with residues in the acceptor Ub contributing to the active site (Baboshina and Haas, 1996; Bremm et al., 2010; Wickliffe et al., 2011). Fourth, UBE2S has a unique disordered *C*-terminal *p*eptide-like "CTP"

extension (Figure 1A) that is multifunctional. UBE2S's CTP binds CDC20 to assemble with APC in a cell-cycle-dependent manner in vivo, binds the APC core to polyubiquitinate substrates, and is subject to autoubiquitination for proteasomal turnover when not engaged in APC-mediated substrate ubiquitination (Garnett et al., 2009; Kelly et al., 2014; Williamson et al., 2009; Wu et al., 2010b). Finally, unlike APC binding to Ub chain-initiating E2s, in vitro interactions between APC and UBE2S are not stimulated by CDH1 and a D-box peptide (Chang et al., 2014). Thus, it is unknown how APC coordinates UBE2S activity with the presence of its Ub-primed substrates.

Despite fundamental importance, mechanisms by which E3s and their Ub chain-elongating E2 partners are functionally linked to drive polyubiquitination remain incompletely understood. Here we address this by taking advantage of our recombinant human APC system (Uzunova et al., 2012). Our study reveals that APC engages and stimulates UBE2S and supports Ub chain elongation in a manner that differs completely from known mechanisms by which canonical RING E3s activate E2s. Instead, APC uses an unprecedented RING-dependent mechanism that increases UBE2S's catalytic efficiency toward forming Ub∼Ub linkages, largely by lowering the apparent K_m (K_m^{app}) for the acceptor Ub. Our data, and complementary work from the Rape lab (Kelly et al., 2014), provide a framework for understanding catalytic features of APC, UBE2S, and RING-mediated polyubiquitination different from heretofore-known E3 elements that activate E2∼Ub intermediates, and that are specialized for Ub chain elongation.

RESULTS

Multiple Atypical E2 Surfaces Dictate UBE2S Specificity and Activation by APC

Polyubiquitination by APC and UBE2S involves the following: (1) E1 generation of the UBE2S∼^{Donor}Ub intermediate, (2) APC and UBE2S interacting, and (3) a catalytic architecture with an acceptor Ub properly placed relative to the UBE2S∼^{Donor}Ub active site (Figure 1B). We identified mechanisms by which APC^{CDH1} harnesses UBE2S in a two-part in vitro assay with 135 purified mutant versions of UBE2S (Figures 1C, S1A, and S1B available online). In the first part, the need for an initiating E2 was bypassed by incorporating a priming acceptor Ub into a fluorescent linear Ub-CyclinB^{NTD*} substrate that is readily polyubiquitinated by APC^{CDH1} and wild-type UBE2S, but not by several of the mutants (Figure S1A). Next, we filtered out defects in E1 charging and catalytic placement of the donor or acceptor Ubs by examining mutational effects on UBE2S autoubiquitination with fluorescent Ub (*Ub), without APC (Figure S1B). Mutations decreasing APC-dependent substrate ubiquitination, but not autoubiquitination, mapped to three UBE2S surfaces, which are remote from the active site and differ from the canonical RING-binding site on an E2 UBC domain: (1) the UBC domain "backside" (R61A/K63A) distal from the active site, (2) the "C" and "D" helices at the C terminus of the UBC domain, and (3) the extreme C terminus of the CTP (Figures 1D, S1A, and S1B). However, because the E2 backside mutant showed increased APC-independent autoubiquitination and no other obvious major defects, we reasoned that its reduced activity in the presence of APC could indirectly arise from self-targeting. Thus, we focused on roles of the other two UBE2S surfaces with APC.

To gain insights into how the different classes of UBE2S mutations impaired their activation by APC, we measured kinetic parameters for APC^{CDH1}-mediated ubiquitination of Ub-CyclinB^{NTD*} while titrating UBE2S concentration (Figures 1E and S1C). Importantly, the K_m^{app} of approximately 78 nM for wild-type UBE2S approaches the roughly 200 nM K_d recently reported for UBE2S binding to APC (Chang et al., 2014). The mutants in the UBC domain C and D helices displayed nearly wild-type K_m^{app} values for UBE2S, but decreased apparent V_{max} (V_{max}^{app}). The helix D (E153A/I154A) mutant was most impaired, with approximately 10-fold decreased V_{max}^{app}. By contrast, the major effect of the CTP L222A mutation was an approximately 9-fold increase in K_m^{app} for UBE2S. Thus, at least two mechanisms couple UBE2S to APC, and one involves binding via the CTP.

Distinctive E2-E3 Interactions: UBE2S CTP Is Recruited to APC Platform even in the Absence of the APC11 RING Domain

To gain insights into interactions, we examined the structure of APC in complex with UBE2S by cryo-electron microscopy (EM) (Figures 2A and S2). Compared to the structure of human APC alone (Chang et al., 2014), extra density was readily visible, which we attribute to UBE2S. Two divergent APC-UBE2S conformers were refined at 13 and 23 Å resolutions, which showed that (1) the APC Platform is flexible, with several orientations of APC4/APC2/APC11 relative to APC1/APC5, and (2) UBE2S occupies various locations, albeit with common features. Fitting UBE2S's UBC domain structure (Sheng et al., 2012) into the maps localized UBE2S as protruding from the Platform region comprising the APC2, APC11, and APC4 subunits and extending toward and contacting APC10.

To localize high-affinity interactions, we tested coimmunoprecipitation of various purified APC assemblies and subcomplexes with FLAG-tagged wild-type and mutant versions of UBE2S (Figures 2B–2D and S2). Mutations in the UBE2S UBC domain, including the backside (R61A/K63A) and C-terminal helix (E153A/I154A), did not affect high-affinity binding to APC (Figure 2B). However, the UBE2S CTP L222A mutant failed to bind recombinant APC (Figure 2C), in agreement with prior studies (Chang et al., 2014; Garnett et al., 2009; Williamson et al., 2009; Wu et al., 2010b). This binding defect explains the increased K_m^{app} value for the UBE2S CTP L222A mutant.

In terms of APC, similar levels of the APC1-APC5-APC4-APC2-APC11 Platform and holo-APC coimmunoprecipitated with FLAG-UBE2S (Figures 2C and S2). This did not require CDC20, CDH1, or substrate. Although the Platform contains APC2-APC11 that might be expected to bind E2s like other cullin-RING ligases, our data suggest distinctive interactions because the isolated APC2-APC11 subcomplex is not sufficient for high-affinity binding, and significant binding was retained upon deleting the APC11 RING domain from the Platform (Figure 2C) and upon codeleting the APC2 C-terminal domain and entire APC11 subunit from the full APC (Figure 2D). However, UBE2S binding was eliminated by codeleting APC11 either with the full APC2 subunit or with APC2's four-helix bundle and

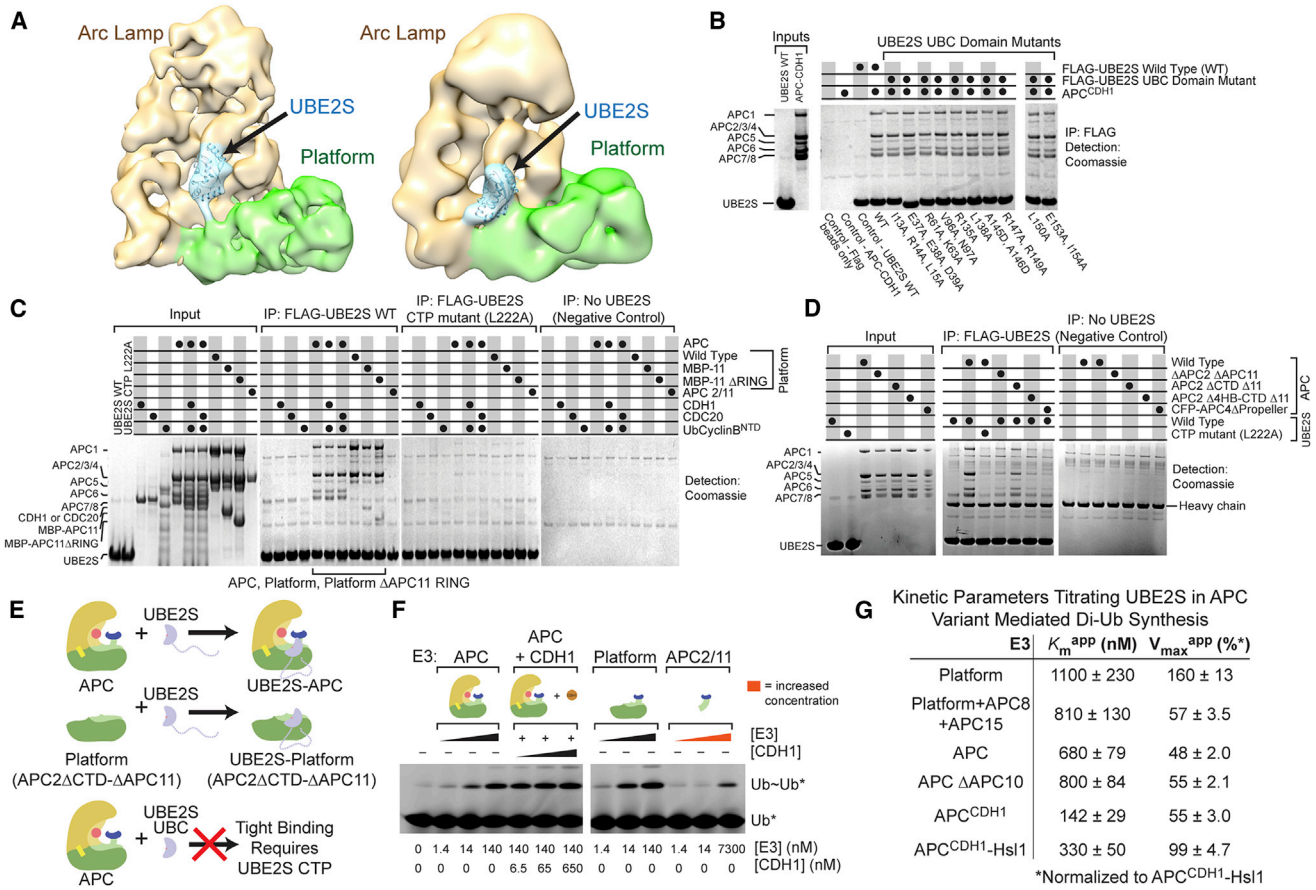

E3	K_m^{app} (nM)	V_{max}^{app} (%*)
Platform	1100 ± 230	160 ± 13
Platform+APC8 +APC15	810 ± 130	57 ± 3.5
APC	680 ± 79	48 ± 2.0
APC ΔAPC10	800 ± 84	55 ± 2.1
APC^{CDH1}	142 ± 29	55 ± 3.0
APC^{CDH1}-Hsl1	330 ± 50	99 ± 4.7

Figure 2. APC Platform and UBE2S CTP Mediate High-Affinity Interactions

(A) EM structures showing two conformations of APC-UBE2S at 13 Å (left) and 23 Å (right) resolution. Platform, green; Arc Lamp, tan; density attributed to UBE2S, cyan with modeled UBC domain.

(B) Coomassie-stained SDS-PAGE showing binding of recombinant APC^{CDH1} with FLAG-UBE2S (WT and UBC domain mutants) after anti-FLAG IP.

(C) As in (B) showing FLAG-UBE2S, but not CTP L222A mutant, coimmunoprecipitates recombinant APC with or without coactivator, and Platform with or without His_6-MBP-APC11 RING (MBP-11 and MBP-11ΔRING). FLAG-UBE2S does not coimmunoprecipitate APC2-APC11 (APC2/11). APC subcomplexes are described in Figure S2.

(D) As in (B) showing FLAG-UBE2S coIP with APC lacking APC2 C-terminal domain and APC11 (APC2ΔCTD Δ11), but not with further deletions of APC2 or a mutant disrupting APC4 structure (CFP-APC4ΔPropeller).

(E) Model summarizing results from (A)–(D). UBE2S CTP is required, and APC Platform is sufficient, for high-affinity APC-UBE2S interaction. From the Platform, APC4 and APC2 four-helix bundle are required for coIP with UBE2S, but APC2 CTD and APC11 are not.

(F) Phosphorimager scans examining effects of indicated APC variants on UBE2S-mediated synthesis of unanchored Ub∼Ub* chains between unlabeled donor Ub and fluorescein-labeled acceptor Ub*. Concentrations of APC variants and CDH1 are indicated.

(G) Kinetic parameters comparing APC^{CDH1} and subcomplexes for recruiting and activating of UBE2S, upon titrating UBE2S concentration in assays monitoring unanchored di-Ub chain synthesis. SEM, n ≥ 3.

See also Figure S2.

C-terminal domain, or by disrupting APC4's β-propeller (Figures 2D and S2). Thus, the APC2-APC4 region of the Platform, near but excluding the APC11 RING, is required for high-affinity binding to UBE2S (Figure 2E).

UBE2S-Mediated Ub Chain Elongation Is Minimally Activated by the Cullin-RING-like APC2-APC11 Subcomplex and Progressively More Enhanced by Platform and APC^{CDH1}

Overall, our data indicated that UBE2S's CTP and the APC Platform confer noncanonical E2-E3 interactions. Thus, we tested if the APC Platform, like APC^{CDH1}, also influences UBE2S activity. Because the isolated Platform lacks ability to recruit a substrate D-box, we could not compare it with APC^{CDH1} for ubiquitinating the Ub-$CyclinB^{NTD*}$ substrate. Instead, we examined effects on UBE2S-mediated transfer of an unlabeled donor Ub to a free fluorescein-labeled acceptor Ub, producing unanchored Ub∼Ub* chains. Di-Ub chain synthesis was efficiently stimulated by adding APC, either alone or with CDH1, or by adding the Platform subcomplex (Figure 2F). However, the isolated APC2-APC11 complex was only able to stimulate UBE2S activity at very high concentration (approximately 70-fold molar excess),

suggesting that other Platform subunits contribute either directly or indirectly to catalysis (Figure 2F).

It was possible to quantitatively compare APC subcomplexes for ability to recruit and activate UBE2S by titrating UBE2S concentration in kinetic assays monitoring di-Ub synthesis (Figures 2G and S1–S3). The Platform subcomplex displayed a K_m^{app} for UBE2S of 1,100 nM and V_{max}^{app} of 160% (normalized to APC^{CDH1}-Hsl1) in synthesizing di-Ub chains. Increasing the number of APC subunits associated with the Platform, such as in a complex containing the Platform, APC8, and APC15, or in the entire APC, led to progressively lower K_m^{app} values for UBE2S. Saturating APC with CDH1 decreased the K_m^{app} for UBE2S to 142 nM during synthesis of free di-Ub chains. This is close to the value of 78 nM for polyubiquitination of Ub-CyclinB^{NTD} (Figure 1E), and is consistent with similar APC-UBE2S interactions in the presence or absence of a D-box substrate. The improved K_m^{app} values for the larger complexes may reflect APC8, APC15, and/or CDH1 influencing the conformation of the Platform, as was observed in a recent EM study (Chang et al., 2014). Also, some subunits in the larger complexes may make direct, but weak, contacts to UBE2S (Kelly et al., 2014; Williamson et al., 2009), or could indirectly stabilize key Platform elements involved in catalysis.

Interestingly, the positive effect of CDH1 on di-Ub synthesis is slightly offset by Hsl1 (Figure 2G), whose D-box tightly engages CDH1 and APC10, but which lacks a priming Ub, and thus is not a direct substrate of UBE2S (Burton et al., 2005; Buschhorn et al., 2011; da Fonseca et al., 2011). Furthermore, deleting APC10 did not substantially influence APC activation of UBE2S-mediated di-Ub synthesis (Figures 2G and S3). These results highlight differences between mechanisms by which APC activates UBE2S versus initiating E2s. As binding to initiating E2s was reportedly stimulated by CDH1, APC10, and D-box substrates (Chang et al., 2014; Van Voorhis and Morgan, 2014), the data led us to consider whether distinct mechanisms establish synergy between APC, UBE2S, and the acceptor Ub.

APC Activates UBE2S-Mediated Ub Chain Synthesis by Lowering K_m^{app} for Acceptor Ub

To investigate roles of APC and UBE2S toward an acceptor Ub, we examined di-Ub synthesis by monitoring transfer of a fluorescein-labeled donor Ub upon titrating unlabeled free acceptor Ub as the substrate, either in the absence or presence of APC^{CDH1} (Figures 3A, S2E, and S2F). Two interesting points emerged from comparing the kinetic parameters for the acceptor Ub substrate between the different reactions. First, there is a striking effect of adding APC^{CDH1}: an approximately 42-fold drop in K_m^{app} for the acceptor Ub and more than a 4-fold increase in V_{max}^{app}. Remarkably, under the conditions of our assay, APC^{CDH1} increased the overall catalytic efficiency of Ub chain synthesis by approximately 175-fold in a manner predominantly mediated through delivery of the acceptor Ub to UBE2S.

Second, measuring kinetic parameters while titrating the acceptor Ub in assays with UBE2S mutants (Figures 3A, 3B, S2E, and S2F) revealed that APC^{CDH1} is almost invisible to both the CTP L222A and helix D E153A I154A mutants. APC's inability to activate the CTP mutant is readily explained by greatly decreased interaction (Figure 2C). However, the helix D E153A/I154A mutant showed substantial interaction with APC by coimmunoprecipitation (Figure 2B) and in kinetic assays titrating UBE2S (Figure 1E; data in Figure 3C). Nonetheless, the UBC domain helix D mutant caused an 11-fold increase in K_m^{app} for the acceptor Ub, and a 4-fold decrease in V_{max}^{app} for synthesizing di-Ub linkages in the presence of APC^{CDH1} (Figure 3A), which we attribute to the I154A substitution (Figure S1A). Thus, the UBC domain helix D mutant can bind to, but is not activated by, APC^{CDH1} in vitro.

UBE2S Helix D "Senses" APC2/APC4 for Activation

We took two approaches to localize regions of APC that activate UBE2S via its helix D. First, we identified a minimal APC subcomplex that stimulates UBE2S-mediated di-Ub synthesis in a helix D-dependent manner. Mutating UBE2S's helix D ablated activation by all APC subcomplexes tested, including very low-level stimulation of di-Ub synthesis by a complex between APC11 and a truncated APC2 encompassing the 4HB and CTD ($APC2^{4HB\text{-}CTD}$) (Figures 3D and S2). Surprisingly, deleting the APC11 RING domain eliminated activation of wild-type UBE2S, and this is explored in separate sections below.

As an orthogonal approach to map interactions with UBE2S helix D, we performed crosslinking (Figure 3E). Amber stop codon suppression technology was used to incorporate the photoactivatable crosslinking amino acid benzoylphenylalanine (BPA) (Chin et al., 2002) into various positions in helix D of FLAG-UBE2S, and into negative control variants that do not bind APC due to deletion of key CTP residues. Crosslinked complexes between UBE2S and APC2 and APC4 were identified in western blots as slower-migrating bands dependent on APC^{CDH1}-UBE2S interaction and UV exposure (Figure 3F). The same results were obtained with APC^{CDH1} in complex with a Ub-Hsl1 substrate, or with the isolated Platform subcomplex, so for simplification, only results for APC^{CDH1} are shown. Together, the data suggested that the APC2/APC4 region of the Platform activates UBE2S by contacting the C-terminal helix of UBC domain.

Evidence for Unprecedented RING Domain Activation of Ub Chain Elongation

We were surprised that deleting the APC11 RING eliminated UBE2S activation by APC2-APC11 (Figure 3D), as the RING does not influence UBE2S coimmunoprecipitation of APC (Figures 2C and 2D), and our saturation mutagenesis did not implicate the surface of UBE2S expected to bind a RING as being important for ubiquitination (Figures 1 and S1A). Thus, we mutationally tested a role for APC11's RING domain in the context of the whole APC. To facilitate detecting stoichiometric incorporation of mutants into recombinant APC, APC11 was expressed with an N-terminal His_6-MBP tag, which did not influence ubiquitination activity (Figure 4). As predicted, deleting the RING domain eliminated Ub-CyclinB^{NTD*} ubiquitination with the initiating E2s UBCH5 and UBCH10. Unexpectedly, however, deleting the APC11 RING domain also eliminated activity with UBE2S (Figure 4).

To test if APC acts as a canonical RING E3 toward UBE2S, we examined effects of Ala substitutions in place of a set of APC11 residues (Arg27, Trp63, and Arg77) that together correspond to anchors in various canonical RING E3-E2~Ub complex

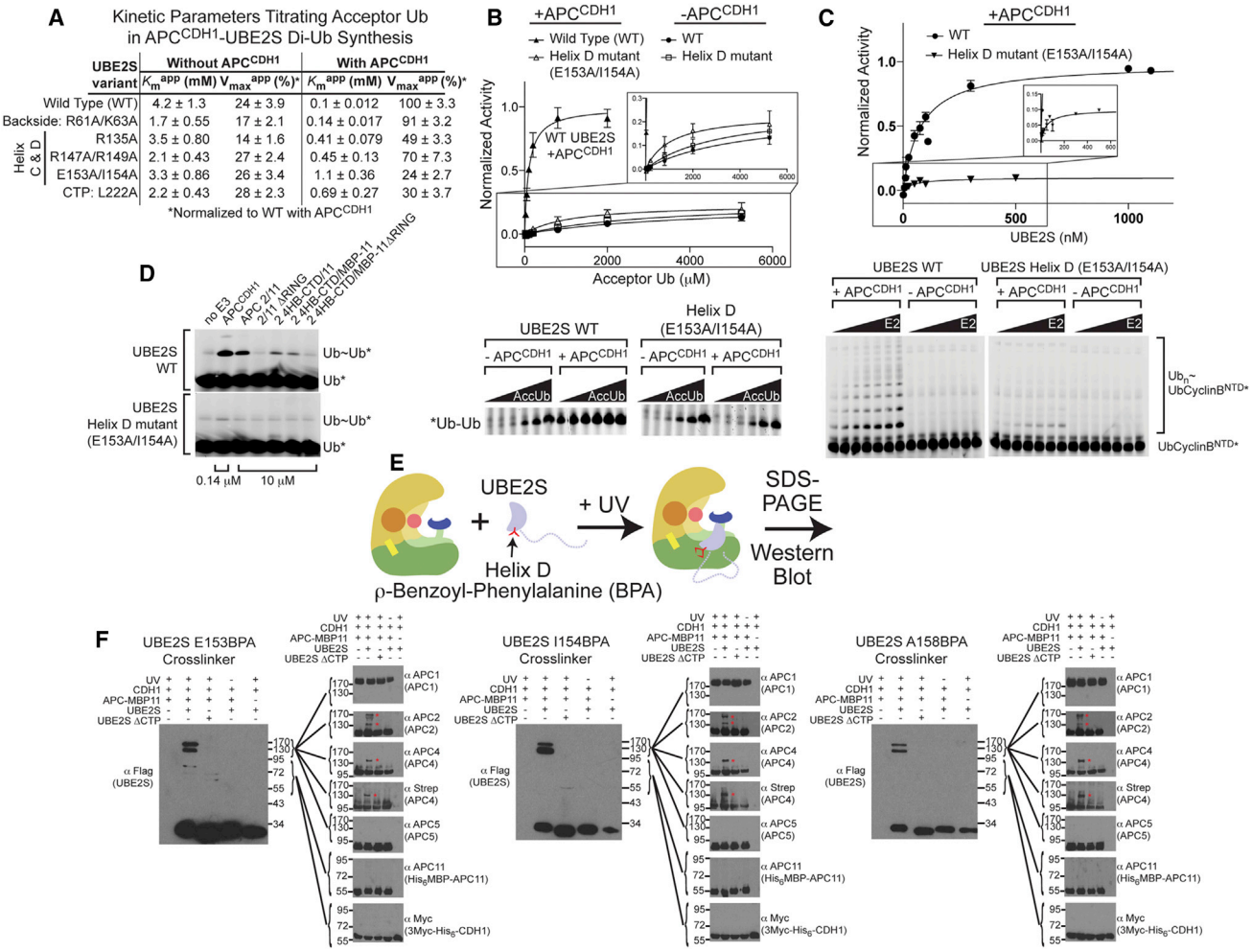

Figure 3. APC Drives PolyUb Chain Formation by Activating a Distinctive Region of the UBE2S UBC Domain and Lowering K_m^{app} for Acceptor Ub

(A) Kinetic parameters from titrating acceptor Ub during di-Ub synthesis, to compare effects of APC^{CDH1} on catalytic efficiency of WT UBE2S or mutants. SEM, $n \geq 3$.

(B) Fits and representative SDS-PAGE for kinetic parameters in Figure 3A, for activity as a function of acceptor Ub concentration, showing APC^{CDH1} activation of di-Ub synthesis by WT UBE2S- and APC^{CDH1}-specific defect for the helix D mutant (E153A/I154A).

(C) Fits and representative SDS-PAGE for kinetic parameters in Figure 1E, showing similar K_m^{app} for WT or helix D mutant UBE2S, in Ub-$CyclinB^{NTD*}$ ubiquitination by APC^{CDH1} measured as a function of UBE2S concentration.

(D) Comparison of APC^{CDH1} or indicated versions of cullin-RING-like APC2-APC11 complex (note 70-fold higher concentration) for activating UBE2S-mediated di-Ub synthesis. Reactions with UBE2S helix D mutant are shown below. APC2/11 subcomplexes are described in Figure S2.

(E) Scheme for photocrosslinking FLAG-UBE2S with BPA (red symbol) in helix D with APC.

(F) Western blots for FLAG-UBE2S or CTP mutant with indicated BPA substitutions, Platform subunits, and CDH1 after photocrosslinking as in Figure 3E. Red asterisks indicate UBE2S-specific crosslinked species observed with APC2 and APC4.

See also Figure S3.

structures (Figure 4) (Dou et al., 2012, 2013; Plechanovová et al., 2012; Pruneda et al., 2012; Scott et al., 2014). None of the canonical RING mutants affected polyubiquitination by UBE2S, despite decreasing ubiquitination with the initiating E2s UBCH5 or UBCH10. The results confirm that APC-mediated Ub chain initiation occurs via a canonical RING mechanism activating UBCH5 or UBCH10, but indicate that the APC11 RING domain contributes to UBE2S-mediated Ub chain elongation in an atypical manner.

Distinctive RING-Dependent Interaction with Acceptor Ub for APC/UBE2S-Mediated Ub Chain Synthesis

To ascertain the function of the RING, APC complexes were purified containing either wild-type His_6-MBP-APC11 or mutants with one to three Ala substitutions in the RING domain (Figures 5 and S4A). The APC RING variants were tested side by side for substrate ubiquitination with UBCH5, UBCH10, and UBE2S (Figure 5A). Mutants showing defects toward all three E2s include a control eliminating zinc-binding cysteines (C23A/C26A/C76A),

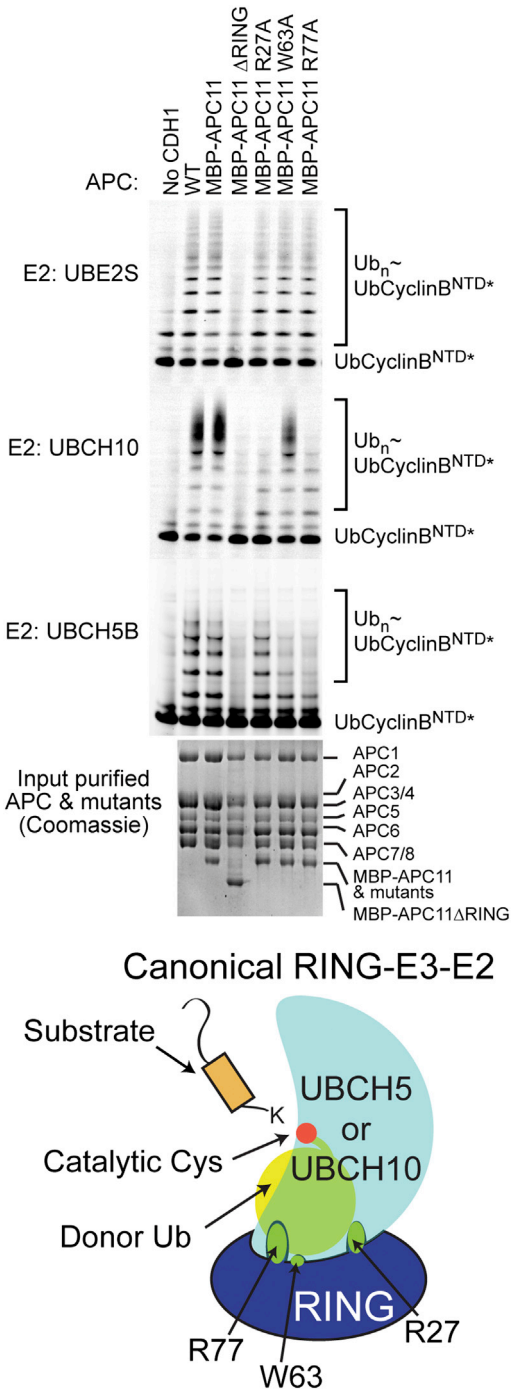

Figure 4. Evidence for Unprecedented RING E3 Mechanism Activating Polyubiquitination by APC-UBE2S

Comparison of Ub-CyclinB^{NTD*} ubiquitination activity for UBE2S, or the initiating E2s UBCH10 or UBCH5, with WT APC^{CDH1} or versions incorporating His$_6$-MBP-APC11 with indicated RING mutations (Δ = deletion; R27A, W63A, R77A = canonical RING-E2~Ub interaction surface as shown in cartoon). Coomassie-stained gel of APC variants shows stoichiometric incorporation of RING variants.

See also Figure S4.

the W16A "pivot" that orients the RING in a cullin-RING ligase, and D42A/D43A that approach a zinc-binding site and presumably influence RING domain stability. There are two other major classes of mutational effects. One class (I25A, R27A, W63A, R77A) maps to the canonical RING surface that binds and activates an E2~Ub intermediate. These are defective toward UBCH5 or UBCH10, but show no effect on UBE2S-mediated ubiquitination. We considered that the high-affinity binding mediated by the UBE2S tail might mask a role for the canonical RING-binding site, but this was not the case; mutations in APC11's canonical E2-binding surface also did not affect ubiquitination with a fragment of UBE2S corresponding to the isolated UBC domain that lacks the CTP, but is still weakly stimulated by APC (Figure 5B).

Intriguingly, the other class of RING mutations (F30A/N31A, M57A, K81A/F82A) preferentially impairs APC-UBE2S-mediated ubiquitination, with little or no effect on UBCH5 or UBCH10 (Figure 5A). Notably, these also impair APC^{CDC20}-mediated ubiquitination of Ub-CyclinB^{NTD*} (Figure S4B), and APC^{CDH1}'s weak activity toward the UBE2S UBC domain (Figure 5B), suggesting a role of the APC11 RING in influencing UBE2S's fundamental catalytic function of generating Ub~Ub linkages. Strikingly, these mutations map to a distinctive surface on the structure of the APC11 RING domain, which we determined by X-ray crystallography and NMR (Figures 5C and S5). Met57 and Phe82 together form an exposed hydrophobic patch on the opposite side of the RING domain from the canonical E2~Ub binding site (Figure 5C). Lys81 is adjacent to the Met57/Phe82 surface. Although Asn31 is exposed, Phe30 is partially buried and supports the structural core that positions Met57. Thus, the F30A mutation may have a localized effect on the structure of Met57 that could explain the preferential loss of activity toward UBE2S, and could also impact RING stability, which may explain its minor effect on UBCH10.

We used the mutants to address how the APC11 RING domain activates UBE2S-mediated Ub chain elongation. In reactions titrating UBE2S and monitoring ubiquitination of Ub-CyclinB^{NTD*}, the distinctive APC11 hydrophobic patch mutants showed little effect on the K_m^{app} for UBE2S, but caused a roughly 2-fold decrease in V_{max}^{app} (Figures 6A and S1G). Moreover, titrating the acceptor Ub in the di-Ub synthesis assay revealed that the distinctive APC11 RING hydrophobic patch mutants substantially increase the K_m^{app} for a free acceptor Ub, with 10- and 16-fold increases for M57A and K81A/F82A, respectively (Figures 6B and S1H). At first glance this profound effect of RING mutants on the K_m^{app} for an acceptor Ub might seem reminiscent of the UBE2S UBC domain E153A/I54A mutant. However, there are differences. The UBE2S mutations appear to affect E2 activation and acceptor Ub interaction, whereas the APC11 RING mutants seem specifically impaired with respect to interacting with an acceptor Ub.

To explore the role of the APC11 RING, we performed NMR and mutational experiments that together are consistent with a mechanism in which the RING domain would recruit an acceptor Ub for UBE2S-mediated chain elongation. First, adding APC2$^{4HB-CTD}$-APC11, which is minimally sufficient to stimulate Ub chain synthesis by UBE2S (Figure 3D), to ^{15}N-labeled Ub caused selective chemical shift perturbations in ^{15}N-^{1}H TROSY spectra

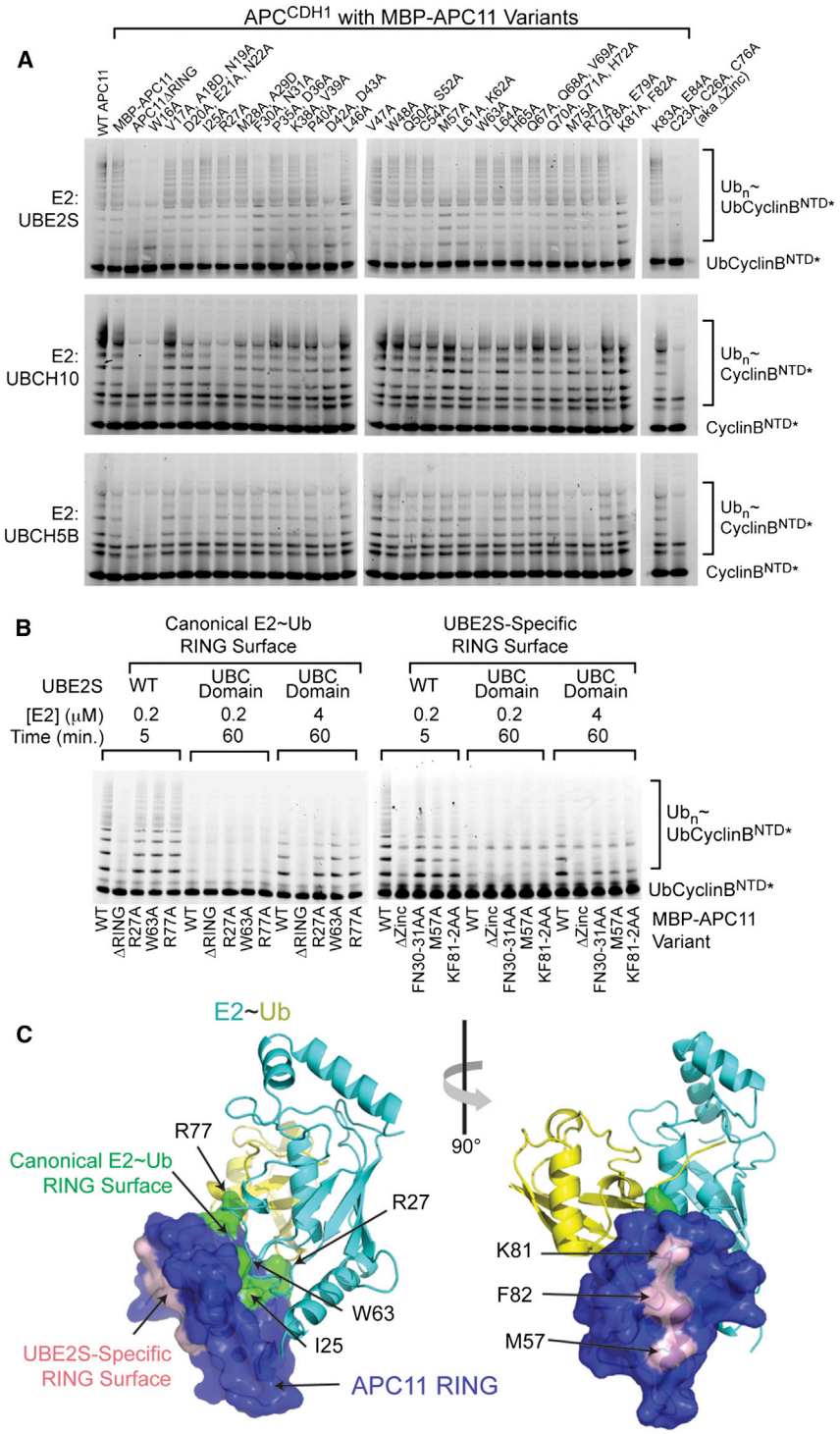

Figure 5. A Distinctive Region of APC11 RING Domain Functions with UBE2S Catalytic UBC Domain to Stimulate Polyubiquitination

(A) Ala-scanning mutagenesis of APC11 RING domain of APC^{CDH1}, comparing mutational effects on ubiquitination by UBE2S, or the initiating E2s UBCH10 or UBCH5, with Ub-CyclinB^{NTD*} or CyclinB^{NTD*} substrates. Confirmation of stoichiometric incorporation of RING variants was enabled by increasing the size of APC11 with a His$_6$-MBP-APC11 for observation by Coomassie gels (data not shown).

(B) Similar mutational profiles for UBE2S and its isolated catalytic UBC domain with Ala mutants in APC11 RING domain of APC^{CDH1}. The indicated high concentrations of UBE2S UBC domain and extended reaction times are required to observe ubiquitination of Ub-CyclinB^{NTD*} by APC^{CDH1} and UBE2S's isolated catalytic UBC domain due to lack of CTP-mediated binding.

(C) UBE2S uses a noncanonical APC11 RING surface. APC11 RING structure (Figure S5) is shown in blue surface, modeled as if in a canonical complex with E2 (cyan)~Ub (yellow) based on a prior RING-UBCH5~Ub structure (Plechanovová et al., 2012). Sites of mutations defective with UBE2S are shown in pink, and with UBCH10 or UBCH5 in green. See also Figure S5.

(Figure 6C). The most strongly shifted resonances map to Ub's Ala46, Lys48, Gln49, His68, and C-terminal region. Notably, this is not the RING-binding surface for the donor Ub in a canonical RING-E2~Ub intermediate (Dou et al., 2012, 2013; Plechanovová et al., 2012; Pruneda et al., 2012). Second, in an experiment performed side by side, there was no effect of adding a mutant APC2$^{4HB-CTD}$-APC11 complex lacking the RING domain (ΔRING) (Figure 6C). Thus, the RING is required for the chemical shift perturbations to Ub. Third, because of the weak interaction, we wished to do a titration experiment. It was necessary to use the isolated APC11 RING domain because we could not obtain high concentrations of the APC2$^{4HB-CTD}$-APC11 complex, produced from insect cells. Although high concentrations were required, titrating the isolated APC11 RING domain progressively shifted the same Ub resonances as APC2$^{4HB-CTD}$-APC11, with predominant effects on Ub's Thr9, Ile13, Arg42, Ala46, Lys48, Gln49, His68, and C-terminal region (Figure 6D). Fourth, in converse experiments, adding unlabeled Ub to ^{15}N-labeled APC11 RING domain revealed selective chemical shift perturbations for Val47 and Glu84 (Figure 6E), which are adjacent to the side chains of Met57 and Phe82 identified in the APC11 Ala scan as critical for reducing the K_m^{app} for the acceptor Ub (Figure S5B). Fifth, given the correlation between NMR and mutagenesis experiments for the APC11 RING, we also performed mutational analysis for the acceptor Ub in UBE2S-catalyzed Ub chain synthesis (Figures 6F and 6G). Acceptor Ub mutants impaired for APC-independent catalysis surround the target Lys11 and correspond to those identified previously (Wickliffe et al., 2011). Importantly, acceptor Ub mutants

A Kinetic Parameters Titrating UBE2S in APC^{CDH1} Ubiquitination of UbCyclinB^{NTD*}

APC variant	K_m^{app} (nM)	V_{max}^{app} (%)*
WT	78 ± 9.7	98 ± 3.9
MBP-APC11	42 ± 9.5	99 ± 6.1
MBP-APC11 (FN30-31AA)	33 ± 9.3	62 ± 4.1
MBP-APC11 (M57A)	55 ± 15	42 ± 2.9
MBP-APC11 (KF81-82AA)	84 ± 27	44 ± 3.9

*Normalized to WT

B Kinetic Parameters Titrating Acceptor Ub in Di-Ub Synthesis by UBE2S/APC^{CDH1}

APC variant	K_m^{app} (mM)	V_{max}^{app} (%)*
WT	0.1 ± 0.012	100 ± 3.3
MBP-APC11	0.089 ± 0.0087	100 ± 2.7
MBP-APC11 (FN30-31AA)	0.36 ± 0.066	77 ± 4.8
MBP-APC11 (M57A)	1.0 ± 0.26	62 ± 7.3
MBP-APC11 (KF81-82AA)	1.6 ± 0.44	55 ± 8.0

*Normalized to WT

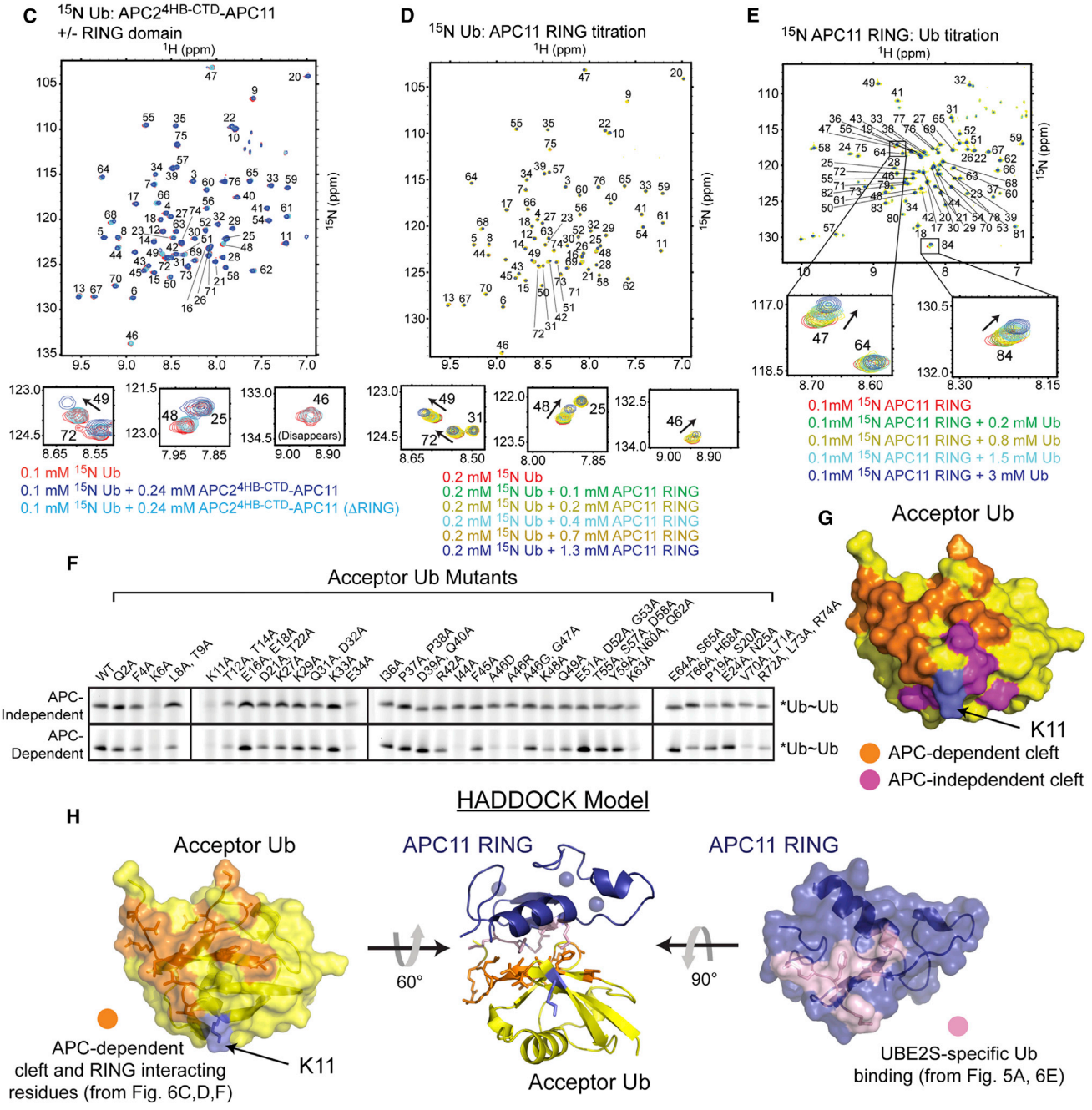

(legend on next page)

with specific defects in APC-dependent ubiquitination map to the RING-binding surface identified by NMR.

To further examine the potential for direct interactions between the APC11 RING and Ub, we generated models based on the NMR data using the program HADDOCK (de Vries et al., 2007). Clustering the 200 resultant models revealed a dominant cluster representing 87% of all docked models. Although the actual interactions may differ in the context of the whole APC-UBE2S complex mediating polyubiquitination, a representative NMR-based HADDOCK model suggests how an acceptor Ub might bind the distinct APC11 hydrophobic patch, and agrees with our mutational data (Figure 6H). Notably, sequence alignments of APC11 across several organisms also show striking correlation between conservation of the RING region (Met57, Lys81, Phe82) that lowers the K_m^{app} for the acceptor Ub and APC's use of UBE2S for polyubiquitination (Figure 7).

DISCUSSION

Distinctive E2 and RING E3 Mechanisms for APC-Mediated Ub Chain Initiation and Elongation

Despite fundamental importance, mechanisms of RING E3-mediated polyubiquitination have remained elusive. Here we show how the critical E3 human APC mediates two-step/two-E2 polyubiquitination through two completely different RING-dependent mechanisms (Figure 7C). APC initiates Ub ligation to substrates by a mechanism involving canonical RING E3 activity, which involves (1) binding a specific substrate motif, (2) the RING domain recruiting an E2∼Ub intermediate and stabilizing the reactive conformation, and (3) crosstalk between the substrate, E2, and E3 to stimulate ligation (Metzger et al., 2014; Scott et al., 2014). APC latches onto substrates via motifs such as a D-box corecruited by CDH1 and APC10, and our mutagenesis showed that the canonical RING E3 surface of APC11 is required with the chain-initiating E2s UBCH5 and UBCH10 (Figures 4 and 5). APC substrates drive their own initial modification, apparently by allosterically modulating APC structure to enhance binding of chain-initiating E2s (Chang et al., 2014; Van Voorhis and Morgan, 2014).

How do RING E3s target a substrate-linked Ub to build a polyUb chain? For APC^{CDH1}, the D-box of a Ub-modified substrate is thought to remain bound to CDH1 and APC10. However, how APC and UBE2S extend the chain on a substrate-linked Ub has been unclear. Surprisingly, we found that APC specifically stimulates Ub chain elongation by recruiting and activating UBE2S by an unexpected multimodal RING-dependent mechanism (Figure 7C). This involves distinctive surfaces from APC and UBE2S, remote from previously defined RING E3-E2∼Ub interaction sites. First, the terminus of UBE2S's flexible CTP is anchored to the APC Platform in a RING-independent manner (Figure 2). This tethers UBE2S to APC, and could facilitate E1 reloading of donor Ub molecules onto APC-bound UBE2S to enhance processive polyubiquitination. Second, helix D from UBE2S's catalytic UBC domain is tweaked by the APC Platform to greatly stimulate polyubiquitination (Figure 3). Although the activation mechanism remains unknown, one possibility may be inferred from regulation of another E2; helix D from the E2 Pex4 binds an allosteric activator to stimulate peroxisomal ubiquitination (Williams et al., 2012) (Figure S6). Alternatively, UBE2S's helix D could coordinate multisite interactions involving the APC2-APC4 region of the Platform, the acceptor Ub, and the APC11 RING. Finally, we showed that APC lowers the K_m of an acceptor Ub reacting with the UBE2S∼Ub intermediate. In addition to APC activation of UBE2S's helix D, this involves the I44/A46/K48/Q49/C-terminal region of the acceptor Ub and, surprisingly, a distinctive hydrophobic patch from the APC11 RING domain. Although it is possible that future studies will show an indirect role for the RING, at this point the simplest explanation for our data would be that during Ub chain elongation, the APC11 RING domain directly captures the substrate-linked acceptor Ub to enhance its interaction with the UBE2S active site, while the APC2-APC4 region recruits and activates UBE2S in proximity (Figures 6 and 7).

Importantly, there is potential for synergy between key features of this mechanism, UBE2S's active site, and the Lys11-linked chains produced and extended on substrates. APC binding to the acceptor Ub could synergize with UBE2S's inherent active site preference for Lys11, by simultaneously directing the acceptor Ub's Lys11 toward the active site and masking Lys48 from serving as an alternative target (Bremm et al., 2010). Furthermore, whereas the I44/A46/K48/Q49/C-terminal region

Figure 6. APC-Mediated Ub Chain Elongation Involves RING Domain Presentation of the Acceptor Ub to UBE2S

(A) UBE2S-specific APC11 RING surface does not recruit UBE2S. Kinetic parameters upon titrating UBE2S in ubiquitination of Ub-Cyclin B^{NTD*}, with WT or indicated APC11 RING mutant versions of APC^{CDH1}. SEM, $n \geq 3$.

(B) UBE2S-specific APC11 RING surface influences interaction with acceptor Ub. Kinetic parameters comparing effects of APC11 RING mutations upon titrating acceptor Ub during APC^{CDH1}-UBE2S-mediated di-Ub synthesis. SEM, $n \geq 3$.

(C) Chemical shift perturbations indicate RING-dependent interactions between Ub and the APC2 4HB-CTD-APC11 subcomplex. TROSY spectra for ^{15}N-labeled Ub alone (red), with $APC2^{4HB-CTD}$-APC11 that can weakly activate Ub-chain synthesis by UBE2S (blue), or a mutant deleted for the RING domain (ΔRING, cyan).

(D) Specific chemical shift perturbations upon titrating the isolated APC11 RING into ^{15}N Ub indicate interaction surface. TROSY spectra for 0.2 mM ^{15}N Ub alone (red), and titration with 0.1, 0.2, 0.4, 0.7, and 1.3 mM APC11 RING domain in green, yellow, cyan, dark yellow, and blue, respectively.

(E) Specific chemical shift perturbations upon titrating Ub into ^{15}N-labeled APC11 RING domain indicate interaction surface. TROSY spectra for 0.1 mM ^{15}N APC11 RING alone in red, and titration with 0.2, 0.8, 1.5, and 3 mM Ub colored green, yellow, cyan, and dark blue, respectively.

(F) Scanning mutagenesis to identify acceptor Ub surface required for APC-dependent UBE2S-mediated di-Ub synthesis. Fluorescent scans of *Ub-Ub chain formation by UBE2S alone (top) or by UBE2S activated with APC^{CDH1} (bottom), with indicated acceptor Ub mutants.

(G) Results from Figure 6F shown on surface of Ub structure. Acceptor Ub residues required for APC-dependent UBE2S-mediated Ub∼Ub chain formation are orange. Acceptor Ub residues required for UBE2S-mediated chain synthesis both with or without APC are magenta, with acceptor Lys11 in purple.

(H) Center; HADDOCK-derived NMR-based model of complex between acceptor Ub (yellow) and APC11 RING (blue). Acceptor Ub residues activated by APC or interacting with APC11 RING identified in Figures 6C, 6D, and 6F are orange, and their localizing to APC11 RING-binding surface is shown on the left. APC11 RING residues activating the acceptor Ub or interacting with Ub identified in Figures 5A and 6E are pink, and their localizing to Ub-binding surface is shown on the right.

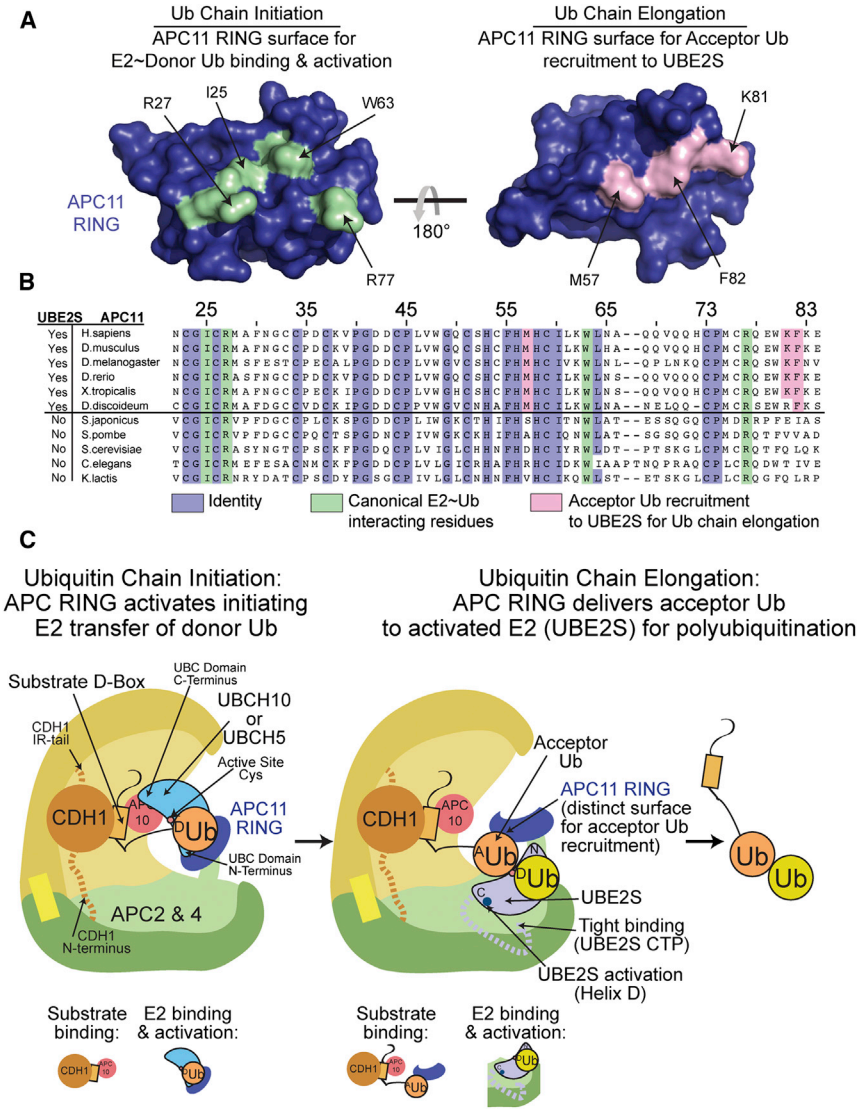

Figure 7. Repurposing the APC RING to Coordinate the Acceptor Ub for Polyubiquitination by Human APC-UBE2S

(A) Separate RING domain surfaces activate Ub chain initiation and elongation by the APC E3. APC11 RING structure is shown as blue surface. Canonical APC11 RING surface activating initiating E2∼Ub intermediate is green. The APC11 RING surface involved in interacting with and presenting the acceptor Ub to UBE2S for chain-elongation maps to the opposite side of the RING domain and is in pink.

(B) Sequence alignment of APC11 RING domain from different organisms, and whether or not UBE2S is present in the organism, shows that APC11 surface mediating acceptor Ub interaction during Ub chain elongation is conserved across organisms where UBE2S is present. Conserved, canonical E2∼Ub-binding, and acceptor Ub-interacting residues are colored slate, green, and pink, respectively.

(C) Model of two-step/two-E2 polyubiquitination by human APC, highlighting dual RING E3 mechanisms. Both Ub chain initiation with a canonical E2 activation mechanism (left) and Ub chain elongation with UBE2S (right) require the APC11 RING domain. In comparison to canonical RING-E2∼Ub mechanisms, human APC activates Ub chain elongation via unique E3-E2 interactions (APC Platform binding UBE2S's C-terminal peptide), distinctive E3 activation of E2 (the APC2/APC4 region activating helix D of UBE2S's UBC domain), and by the APC11 RING coordinating the acceptor Ub with UBE2S.

Related to Figure S6.

of Ub is buried in di-Ub chains with some other linkages, this surface is exposed in Lys11-linked chains (Bremm et al., 2010). Thus, as a Lys11-linked chain grows on a substrate, the I44/A46/K48/Q49/C-terminal surface of the distal Ub is available to bind APC for delivery of its Lys11 to UBE2S's active site.

APC Increasing UBE2S Access to the Acceptor Ub Could Massively Increase Polyubiquitination

The importance of enhancing UBE2S access to an acceptor Ub is underscored by results of an earlier study performed without knowledge of the APC mechanism, where tethering UBE2S's catalytic UBC domain to a heterologous Ub-binding domain increased formation of polyUb chains (Bremm et al., 2010). APC achieves this function naturally, by multiple elements converging to increase interactions between the UBE2S∼Ub intermediate and the acceptor Ub, manifested as an approximately 40-fold decrease in K_m^{app} for a free acceptor Ub and an overall approximately 175-fold increase in catalytic efficiency under the conditions of our assay (Figure 3A).

In the context of a highly interconnected APC-coactivator-substrate∼^{Acceptor}Ub-UBE2S∼^{Donor}Ub complex, avidity effects that culminate in bringing an acceptor Ub to the active site could massively stimulate polyubiquitination in many ways. The accompanying study by Rape and coworkers shows that APC binding to an acceptor Ub can serve as a means to track the acceptor at the tip of a single Ub chain growing on a substrate (Kelly et al., 2014). Indeed, we found that deleting the APC11 RING domain, which is required for lowering the K_m for a free acceptor Ub, completely eliminated generation of a chain on the Ub-CyclinB^{NTD*} substrate (Figure 4). Interestingly, point mutations in the RING domain that partially impair acceptor Ub interaction caused a striking loss of long chains on Ub-CyclinB^{NTD*} in qualitative assays (Figures 5A and 5B). Although future studies will be required to determine the precise basis for this effect, one possibility is that APC^{CDH1} binding to both a D-box and to an acceptor Ub could increase the residence time of Ub-modified substrates on APC, thereby enhancing processivity of UBE2S-mediated polyubiquitination. It is also possible that the position of an acceptor Ub influences its capture by APC, with preferential effects on long chain formation in the context of

the Ub-CyclinB^{NTD*} substrate. More complicated scenarios may arise with natural substrates that are initially decorated with multiple individual Ub molecules (Dimova et al., 2012). Here APC may preferentially guide a particular priming Ub to the UBE2S active site, and essentially recapture the tip of one selected chain as it grows. At some point, the length of a given chain may exceed topological constraints for the substrate to remain anchored to a coactivator and APC10, and for the acceptor Ub to simultaneously engage the APC11 RING and UBE2S's active site. When the optimal length is exceeded for one chain, another substrate-linked Ub may be preferentially guided for extension by APC/UBE2S. As a result, multiple Ub chains may ultimately be produced on a substrate. In the context of the cellular milieu, the APC-Ub interaction could also protect a growing chain and prevent its premature disassembly or degradation by blocking access of deubiquitinating enzymes, proteasome receptors, or other destabilizing Ub-binding machineries. Thus, by delivering the acceptor Ub to UBE2S, the distinctive APC RING mechanism would influence the linkage, length, nature, positions, and density of polyUb chains on a substrate, with the net effect of driving proteasomal turnover of cell-cycle regulatory proteins to control cell division.

Implications of APC/UBE2S Mechanism for Cell-Cycle Regulation

The distinct mechanism of APC/UBE2S-mediated Ub chain elongation may contribute to ordering of events during the cell cycle. A prior study indicated that APC substrates processively modified by chains in a single binding event are degraded earlier in mitosis compared to those substrates needing more cycles of APC binding to receive multiple Ubs (Rape et al., 2006). In a related vein, substrates modified by UBE2S are likely more extensively modified with polyUb chains. Thus, substrates that require long Ub chains for proteasomal turnover might be degraded only during phases of the cell cycle when UBE2S is most active (Dimova et al., 2012; Matsumoto et al., 2010).

UBE2S activity in vivo is positively regulated by assembly with APC in a CDC20-dependent manner (Kelly et al., 2014), and inhibited by EMI1 and EMI2 mimicking UBE2S's CTP and impeding Ub chain elongation during interphase and meiosis, respectively (Frye et al., 2013; Sako et al., 2014; Wang and Kirschner, 2013). It is conceivable that EMI1/EMI2 inhibition could also involve blocking the distinctive APC11 RING surface and acceptor Ub interaction. Timing is further influenced by autocatalytic Ub-dependent proteolysis of UBE2S (Garnett et al., 2009; Rape and Kirschner, 2004; Williamson et al., 2009; Wu et al., 2010b). Notably, the accompanying work suggests UBE2S specifically regulates inactivation of the spindle assembly checkpoint (Kelly et al., 2014). Future studies will be required to identify key roles of APC/UBE2S-generated Lys11-linked polyUb chains in the checkpoint and other aspects of cell-cycle regulation.

General Implications for RING E3-E2-Mediated Polyubiquitination

Acceptor Ub recruitment and/or positioning is emerging as a fundamental component of RING-E3-E2-mediated polyubiquitination. Prior studies showed potential for the acceptor Ub to be recruited by domains embedded within E2s or their partners, or by specialized polyubiquitinating E4 enzymes (Choi et al., 2010; Eddins et al., 2006; Koegl et al., 1999; Liu et al., 2014; Spratt and Shaw, 2011). Even the chain-elongating E2 functioning with yeast APC, Ubc1, which is thought to be activated by a canonical RING mechanism, can recruit Ub via its own UBA domain (Merkley and Shaw, 2004). During evolution and transfer of chain-elongating activity to UBE2S, the job of acceptor Ub recruitment apparently was shifted to APC. RING domain repurposing may be an ideal mechanism for recruiting an acceptor Ub. Indeed, with its location adjacent to the catalytic center, and the notorious ability of RING domains to rotate relative to the rest of E3 enzymes (Duda et al., 2008), the APC11 RING domain may be ideally poised to capture a terminal Ub immediately after its ligation (Figures 7A and 7B).

It is appealing to speculate that the APC11 RING serves as a hub to integrate Ub chain initiation and elongation (Williamson et al., 2009). Although we do not have any evidence for cooperativity between UBCH10 and UBE2S, this is in principle possible based on mutagenic and NMR studies showing separation between the canonical RING site for E2∼Ub activation and the surface delivering the acceptor Ub to UBE2S (Figures 5 and 6). Future studies will be required to determine if, how, when, and why the two steps of Ub chain formation by APC occur simultaneously or synergistically.

At this point, we do not know if other E3s utilize their RING domains to deliver an acceptor Ub to the E2 for polyubiquitination. Nonetheless, our findings with APC and UBE2S expand our knowledge of RING E3 and E2 mechanisms. We speculate that future studies will show that some of the massive number of RING proteins associated with Ub pathways have alternative functions like human APC, providing specialized points regulating ubiquitination.

EXPERIMENTAL PROCEDURES

Other than yeast Hsl1, proteins are human and were expressed and purified for enzyme and interaction assays, NMR, and EM largely as described (Frye et al., 2013), with some alterations. In particular, recombinant APC was purified to greater homogeneity by a protocol similar to that used by Chang et al. (2014), with affinity purification based on a C-terminal Twin-Strep tag on APC4, followed by anion exchange chromatography and gel filtration. Although our previous protocol for purifying recombinant APC led to a K_m for UBE2S in Ub-CyclinB^{NTD*} ubiquitination assays (Frye et al., 2013) that matched well to values obtained in similar reactions with endogenous APC (Wang and Kirschner, 2013), we attribute improved catalytic efficiency herein to improved homogeneity from our revised APC purification scheme.

NMR and crystallography were performed much as described previously (Duda et al., 2008; Frye et al., 2013) (Tables 1 and 2). Samples for cryo-EM were prepared using the Grafix protocol (Kastner et al., 2008), blotted, and vitrified (Vitrobot, FEI Company). Images were recorded at a magnification of 74,000× (2 Å/pixel) under cryogenic conditions in a C_s corrected Titan Krios (FEI Company) electron microscope on a Falcon II Direct Electron Detector (FEI Company).

For UBE2S-APC coimmunoprecipitation binding assays, APC complexes and UBE2S variants were mixed at concentrations of 0.1 μM and 6 μM, respectively, with anti-FLAG M2 affinity gel (Sigma) in 20 mM HEPES (pH 8.0), 200 mM NaCl, 0.25 mg/ml BSA, and 0.1% Tween 20. After 3 hr of gentle mixing, the beads were washed repeatedly with cycles of resuspending in buffer, spinning down beads, and rewashing prior to adding SDS gel-loading buffer to the beads. The samples were then boiled and analyzed by SDS-PAGE and Coomassie staining.

Enzyme assays were performed largely as described previously (Frye et al., 2013). In the figures, the position of the * indicates the position of the

Table 1. Crystallographic Data and Refinement Statistics

Data Collection	
Wavelength (λ)	1.2827
Space group	$P2_1$
Unit Cell Parameters	
a, b, c (Å)	52.45, 39.88, 65.04
α, β, ϒ (°)	90.00, 108.49, 90.00
Resolution (Å)	61.58–1.76
No. of measured reflections	123,853
No. of unique reflections	24,444
Overall R_{sym} (%)	5.5 (16.7)
Completeness (%)	95.1 (80.2)
Overall I/σI	24.0 (7.6)
Mean redundancy	5.1
Refinement	
R_{work}/R_{free}	0.192/0.229
rmsd bond lengths (Å)	0.008
rmsd bond angles (°)	1.2
Subunits in asymmetric unit	4
No. of Atoms	
Protein	2,030
Zinc	12
Water	166
Ramachandran Statistics	
Residues in most favored regions (%)	98.3
Residues in disallowed regions (%)	0.0

Highest-resolution shell is shown in parentheses. R_{free} is the cross-validation of R factor, with > 8% of the total reflections omitted in model refinement.

Table 2. Statistics for the NMR Structure Calculation of APC11 RING

Constraints	
No. of upper distance limits	1,033
Intraresidue	408
Short range ($\|i–j\| \leq 1$)	260
Medium range ($2 \leq \|i–j\| \geq 5$)	118
Long range ($5 < \|i–j\|$)	247
Zinc restraints	12
No. of dihedral angle constraints	32
No. of hydrogen bonds	18
Residual target function ($Å^2$)	0.33 ± 0.04
Distance Violations > 0.2 Å	
Minimum violation (Å)	0.02 ± 0.004
Maximum violation (Å)	0.03 ± 0.004
Angle Violation (°)	
Minimum	0.04 ± 0.03
Maximum	0.14 ± 0.03
Atomic Pairwise rmsd (Å)[a]	
Backbone atoms	0.42 ± 0.08
Heavy atoms	1.01 ± 0.01
Structural Analysis	
Residues in allowed region (%)	98.3
Residues in generously allowed region (%)	1.7
Residues in disallowed region (%)	0.0

[a]Backbone and heavy atom rmsds are obtained by superimposing residues 8–15 and 30–70 of the APC11 RING. Residues 1–6 and 16–30 did not show any long-range NOEs and hence were unstructured. Backbone heavy atom rmsd for 3–70 is 1.07 ± 0.2.

fluorescent label on a substrate, with * before the name indicating an N-terminal label and * after the name indicating a C-terminal label. The assays measuring enzyme kinetics of APC-dependent ubiquitination have two substrates, the UBE2S~^{Donor}Ub intermediate and the substrate being modified by the donor Ub, which here was either Ub-CyclinB^{NTD*} or various versions of free Ub optimal for observing di-Ub synthesis in the different conditions. Thus, titrating UBE2S concentrations yielded kinetic constants for UBE2S, and titrating free acceptor Ub yielded kinetic constants for the acceptor Ub.

Detailed experimental procedures are provided in Supplemental Information.

ACCESSION NUMBERS

The accession numbers for the data reported in this paper are 4R2Y.pdb, 2MT5.pdb, BMRB-25149, EMD-2775, and EMD-6084.

SUPPLEMENTAL INFORMATION

Supplemental Information includes six figures and Supplemental Experimental Procedures and can be found with this article online at http://dx.doi.org/10.1016/j.molcel.2014.09.009.

AUTHOR CONTRIBUTIONS

E.R.W., F.W., and M.A.J. contributed equally to this work. N.G.B., B.A.S., J.-M.P., and H.S. planned and supervised the project. N.G.B., E.R.W., M.A.J., R.Q., and I.F.D. performed biochemical and biophysical analyses. F.W., R.V., G.P., and J.J.F. developed the recombinant APC system used here. N.G.B. and R.V. prepared EM samples. H.S. performed EM with help from P.D. NMR analyses were performed by N.G.B. and C.R.R.G. Samples were prepared by N.G.B., S.E.C., and O.A. for biochemical and biophysical studies. A.N. performed AUC. J.B. and J.J.Z. performed HADDOCK modeling. N.G.B., O.A., and I.K. performed X-ray crystallography. N.G.B., J.J.F., E.R.W., H.S., and B.A.S. prepared the manuscript with input from all authors.

ACKNOWLEDGMENTS

We thank M. Rape and colleagues for communicating results prior to publication; K.P. Wu, A. Dick, and D. Gerlich for advice, discussions, and collaboration; and S. Bozeman, D.W. Miller, and J. Bollinger for support. For funding, we thank the Jane Coffin Childs Foundation (N.G.B.); Deutsche Forschungsgemeinschaft Sonderforschungsbereich 860 (H.S.); Boehringer Ingelheim, the Laura Bassi Centre for Optimized Structural Studies, EU-FP7 grant no. 227764 MitoSys, and the Austrian Research Fund (J.-M.P.); ALSAC, NIH R37GM065930 and P30CA021765, and HHMI (B.A.S.); R01GM100909 (J.JZ.); and NIH P41GM103403 and DOE DE-AC02-06CH11357 (NECAT and APS). B.A.S. is an Investigator of the Howard Hughes Medical Institute.

Received: July 21, 2014
Revised: August 29, 2014
Accepted: September 3, 2014
Published: October 9, 2014

REFERENCES

Baboshina, O.V., and Haas, A.L. (1996). Novel multiubiquitin chain linkages catalyzed by the conjugating enzymes E2EPF and RAD6 are recognized by 26 S proteasome subunit 5. J. Biol. Chem. *271*, 2823–2831.

Berndsen, C.E., Wiener, R., Yu, I.W., Ringel, A.E., and Wolberger, C. (2013). A conserved asparagine has a structural role in ubiquitin-conjugating enzymes. Nat. Chem. Biol. *9*, 154–156.

Bremm, A., Freund, S.M., and Komander, D. (2010). Lys11-linked ubiquitin chains adopt compact conformations and are preferentially hydrolyzed by the deubiquitinase Cezanne. Nat. Struct. Mol. Biol. *17*, 939–947.

Burton, J.L., Tsakraklides, V., and Solomon, M.J. (2005). Assembly of an APC-Cdh1-substrate complex is stimulated by engagement of a destruction box. Mol. Cell *18*, 533–542.

Buschhorn, B.A., Petzold, G., Galova, M., Dube, P., Kraft, C., Herzog, F., Stark, H., and Peters, J.M. (2011). Substrate binding on the APC/C occurs between the coactivator Cdh1 and the processivity factor Doc1. Nat. Struct. Mol. Biol. *18*, 6–13.

Chang, L., Zhang, Z., Yang, J., McLaughlin, S.H., and Barford, D. (2014). Molecular architecture and mechanism of the anaphase-promoting complex. Nature *513*, 388–393.

Chin, J.W., Martin, A.B., King, D.S., Wang, L., and Schultz, P.G. (2002). Addition of a photocrosslinking amino acid to the genetic code of *Escherichiacoli*. Proc. Natl. Acad. Sci. USA *99*, 11020–11024.

Choi, Y.S., Wu, K., Jeong, K., Lee, D., Jeon, Y.H., Choi, B.S., Pan, Z.Q., Ryu, K.S., and Cheong, C. (2010). The human Cdc34 carboxyl terminus contains a non-covalent ubiquitin binding activity that contributes to SCF-dependent ubiquitination. J. Biol. Chem. *285*, 17754–17762.

da Fonseca, P.C., Kong, E.H., Zhang, Z., Schreiber, A., Williams, M.A., Morris, E.P., and Barford, D. (2011). Structures of APC/C(Cdh1) with substrates identify Cdh1 and Apc10 as the D-box co-receptor. Nature *470*, 274–278.

de Vries, S.J., van Dijk, A.D., Krzeminski, M., van Dijk, M., Thureau, A., Hsu, V., Wassenaar, T., and Bonvin, A.M. (2007). HADDOCK versus HADDOCK: new features and performance of HADDOCK2.0 on the CAPRI targets. Proteins *69*, 726–733.

Dimova, N.V., Hathaway, N.A., Lee, B.H., Kirkpatrick, D.S., Berkowitz, M.L., Gygi, S.P., Finley, D., and King, R.W. (2012). APC/C-mediated multiple monoubiquitylation provides an alternative degradation signal for cyclin B1. Nat. Cell Biol. *14*, 168–176.

Dou, H., Buetow, L., Sibbet, G.J., Cameron, K., and Huang, D.T. (2012). BIRC7-E2 ubiquitin conjugate structure reveals the mechanism of ubiquitin transfer by a RING dimer. Nat. Struct. Mol. Biol. *19*, 876–883.

Dou, H., Buetow, L., Sibbet, G.J., Cameron, K., and Huang, D.T. (2013). Essentiality of a non-RING element in priming donor ubiquitin for catalysis by a monomeric E3. Nat. Struct. Mol. Biol. *20*, 982–986.

Dube, P., Herzog, F., Gieffers, C., Sander, B., Riedel, D., Müller, S.A., Engel, A., Peters, J.M., and Stark, H. (2005). Localization of the coactivator Cdh1 and the cullin subunit Apc2 in a cryo-electron microscopy model of vertebrate APC/C. Mol. Cell *20*, 867–879.

Duda, D.M., Borg, L.A., Scott, D.C., Hunt, H.W., Hammel, M., and Schulman, B.A. (2008). Structural insights into NEDD8 activation of cullin-RING ligases: conformational control of conjugation. Cell *134*, 995–1006.

Eddins, M.J., Carlile, C.M., Gomez, K.M., Pickart, C.M., and Wolberger, C. (2006). Mms2-Ubc13 covalently bound to ubiquitin reveals the structural basis of linkage-specific polyubiquitin chain formation. Nat. Struct. Mol. Biol. *13*, 915–920.

Frye, J.J., Brown, N.G., Petzold, G., Watson, E.R., Grace, C.R., Nourse, A., Jarvis, M.A., Kriwacki, R.W., Peters, J.M., Stark, H., and Schulman, B.A. (2013). Electron microscopy structure of human APC/C(CDH1)-EMI1 reveals multimodal mechanism of E3 ligase shutdown. Nat. Struct. Mol. Biol. *20*, 827–835.

Garnett, M.J., Mansfeld, J., Godwin, C., Matsusaka, T., Wu, J., Russell, P., Pines, J., and Venkitaraman, A.R. (2009). UBE2S elongates ubiquitin chains on APC/C substrates to promote mitotic exit. Nat. Cell Biol. *11*, 1363–1369.

Herzog, F., Primorac, I., Dube, P., Lenart, P., Sander, B., Mechtler, K., Stark, H., and Peters, J.M. (2009). Structure of the anaphase-promoting complex/cyclosome interacting with a mitotic checkpoint complex. Science *323*, 1477–1481.

Kastner, B., Fischer, N., Golas, M.M., Sander, B., Dube, P., Boehringer, D., Hartmuth, K., Deckert, J., Hauer, F., Wolf, E., et al. (2008). GraFix: sample preparation for single-particle electron cryomicroscopy. Nat. Methods *5*, 53–55.

Kelly, A., Wickliffe, K.E., Song, L., Fedrigo, I., and Rape, M. (2014). Ubiquitin chain elongation requires E3-dependent tracking of the emerging conjugate. Mol. Cell *56*, this issue, 232–245.

Kimata, Y., Baxter, J.E., Fry, A.M., and Yamano, H. (2008). A role for the Fizzy/Cdc20 family of proteins in activation of the APC/C distinct from substrate recruitment. Mol. Cell *32*, 576–583.

Koegl, M., Hoppe, T., Schlenker, S., Ulrich, H.D., Mayer, T.U., and Jentsch, S. (1999). A novel ubiquitination factor, E4, is involved in multiubiquitin chain assembly. Cell *96*, 635–644.

Liu, W., Shang, Y., Zeng, Y., Liu, C., Li, Y., Zhai, L., Wang, P., Lou, J., Xu, P., Ye, Y., and Li, W. (2014). Dimeric Ube2g2 simultaneously engages donor and acceptor ubiquitins to form Lys48-linked ubiquitin chains. EMBO J. *33*, 46–61.

Matsumoto, M.L., Wickliffe, K.E., Dong, K.C., Yu, C., Bosanac, I., Bustos, D., Phu, L., Kirkpatrick, D.S., Hymowitz, S.G., Rape, M., et al. (2010). K11-linked polyubiquitination in cell cycle control revealed by a K11 linkage-specific antibody. Mol. Cell *39*, 477–484.

Mattiroli, F., and Sixma, T.K. (2014). Lysine-targeting specificity in ubiquitin and ubiquitin-like modification pathways. Nat. Struct. Mol. Biol. *21*, 308–316.

Merkley, N., and Shaw, G.S. (2004). Solution structure of the flexible class II ubiquitin-conjugating enzyme Ubc1 provides insights for polyubiquitin chain assembly. J. Biol. Chem. *279*, 47139–47147.

Metzger, M.B., Pruneda, J.N., Klevit, R.E., and Weissman, A.M. (2014). RING-type E3 ligases: master manipulators of E2 ubiquitin-conjugating enzymes and ubiquitination. Biochim. Biophys. Acta *1843*, 47–60.

Plechanovová, A., Jaffray, E.G., Tatham, M.H., Naismith, J.H., and Hay, R.T. (2012). Structure of a RING E3 ligase and ubiquitin-loaded E2 primed for catalysis. Nature *489*, 115–120.

Primorac, I., and Musacchio, A. (2013). Panta rhei: the APC/C at steady state. J. Cell Biol. *201*, 177–189.

Pruneda, J.N., Littlefield, P.J., Soss, S.E., Nordquist, K.A., Chazin, W.J., Brzovic, P.S., and Klevit, R.E. (2012). Structure of an E3:E2~Ub complex reveals an allosteric mechanism shared among RING/U-box ligases. Mol. Cell *47*, 933–942.

Rape, M., and Kirschner, M.W. (2004). Autonomous regulation of the anaphase-promoting complex couples mitosis to S-phase entry. Nature *432*, 588–595.

Rape, M., Reddy, S.K., and Kirschner, M.W. (2006). The processivity of multiubiquitination by the APC determines the order of substrate degradation. Cell *124*, 89–103.

Reverter, D., and Lima, C.D. (2005). Insights into E3 ligase activity revealed by a SUMO-RanGAP1-Ubc9-Nup358 complex. Nature *435*, 687–692.

Rodrigo-Brenni, M.C., and Morgan, D.O. (2007). Sequential E2s drive polyubiquitin chain assembly on APC targets. Cell *130*, 127–139.

Saha, A., Lewis, S., Kleiger, G., Kuhlman, B., and Deshaies, R.J. (2011). Essential role for ubiquitin-ubiquitin-conjugating enzyme interaction in ubiquitin discharge from Cdc34 to substrate. Mol. Cell *42*, 75–83.

Sako, K., Suzuki, K., Isoda, M., Yoshikai, S., Senoo, C., Nakajo, N., Ohe, M., and Sagata, N. (2014). Emi2 mediates meiotic MII arrest by competitively inhibiting the binding of Ube2S to the APC/C. Nat. Commun. *5*, 3667.

Schreiber, A., Stengel, F., Zhang, Z., Enchev, R.I., Kong, E.H., Morris, E.P., Robinson, C.V., da Fonseca, P.C., and Barford, D. (2011). Structural basis

for the subunit assembly of the anaphase-promoting complex. Nature *470*, 227–232.

Scott, D.C., Sviderskiy, V.O., Monda, J.K., Lydeard, J.R., Cho, S.E., Harper, J.W., and Schulman, B.A. (2014). Structure of a RING E3 trapped in action reveals ligation mechanism for the ubiquitin-like protein NEDD8. Cell *157*, 1671–1684.

Sheng, Y., Hong, J.H., Doherty, R., Srikumar, T., Shloush, J., Avvakumov, G.V., Walker, J.R., Xue, S., Neculai, D., Wan, J.W., et al. (2012). A human ubiquitin conjugating enzyme (E2)-HECT E3 ligase structure-function screen. Mol. Cell. Proteomics *11*, 329–341.

Spratt, D.E., and Shaw, G.S. (2011). Association of the disordered C-terminus of CDC34 with a catalytically bound ubiquitin. J. Mol. Biol. *407*, 425–438.

Uzunova, K., Dye, B.T., Schutz, H., Ladurner, R., Petzold, G., Toyoda, Y., Jarvis, M.A., Brown, N.G., Poser, I., Novatchkova, M., et al. (2012). APC15 mediates CDC20 autoubiquitylation by APC/C(MCC) and disassembly of the mitotic checkpoint complex. Nat. Struct. Mol. Biol. *19*, 1116–1123.

Van Voorhis, V.A., and Morgan, D.O. (2014). Activation of the APC/C ubiquitin ligase by enhanced E2 efficiency. Curr. Biol. *24*, 1556–1562.

Wang, W., and Kirschner, M.W. (2013). Emi1 preferentially inhibits ubiquitin chain elongation by the anaphase-promoting complex. Nat. Cell Biol. *15*, 797–806.

Wickliffe, K.E., Lorenz, S., Wemmer, D.E., Kuriyan, J., and Rape, M. (2011). The mechanism of linkage-specific ubiquitin chain elongation by a single-subunit E2. Cell *144*, 769–781.

Williams, C., van den Berg, M., Panjikar, S., Stanley, W.A., Distel, B., and Wilmanns, M. (2012). Insights into ubiquitin-conjugating enzyme/ co-activator interactions from the structure of the Pex4p:Pex22p complex. EMBO J. *31*, 391–402.

Williamson, A., Wickliffe, K.E., Mellone, B.G., Song, L., Karpen, G.H., and Rape, M. (2009). Identification of a physiological E2 module for the human anaphase-promoting complex. Proc. Natl. Acad. Sci. USA *106*, 18213–18218.

Wu, K., Kovacev, J., and Pan, Z.Q. (2010a). Priming and extending: a UbcH5/Cdc34 E2 handoff mechanism for polyubiquitination on a SCF substrate. Mol. Cell *37*, 784–796.

Wu, T., Merbl, Y., Huo, Y., Gallop, J.L., Tzur, A., and Kirschner, M.W. (2010b). UBE2S drives elongation of K11-linked ubiquitin chains by the anaphase-promoting complex. Proc. Natl. Acad. Sci. USA *107*, 1355–1360.

Molecular Cell, Volume *56*

Supplemental Information

Mechanism of Polyubiquitination by Human Anaphase-Promoting Complex: RING Repurposing for Ubiquitin Chain Assembly

Nicholas G. Brown, Edmond R. Watson, Florian Weissmann, Marc A. Jarvis, Ryan VanderLinden, Christy R. R. Grace, Jeremiah J. Frye, Renping Qiao, Prakash Dube, Georg Petzold, Shein Ei Cho, Omar Alsharif, Ju Bao, Iain F. Davidson, Jie J. Zheng, Amanda Nourse, Igor Kurinov, Jan-Michael Peters, Holger Stark, and Brenda A. Schulman

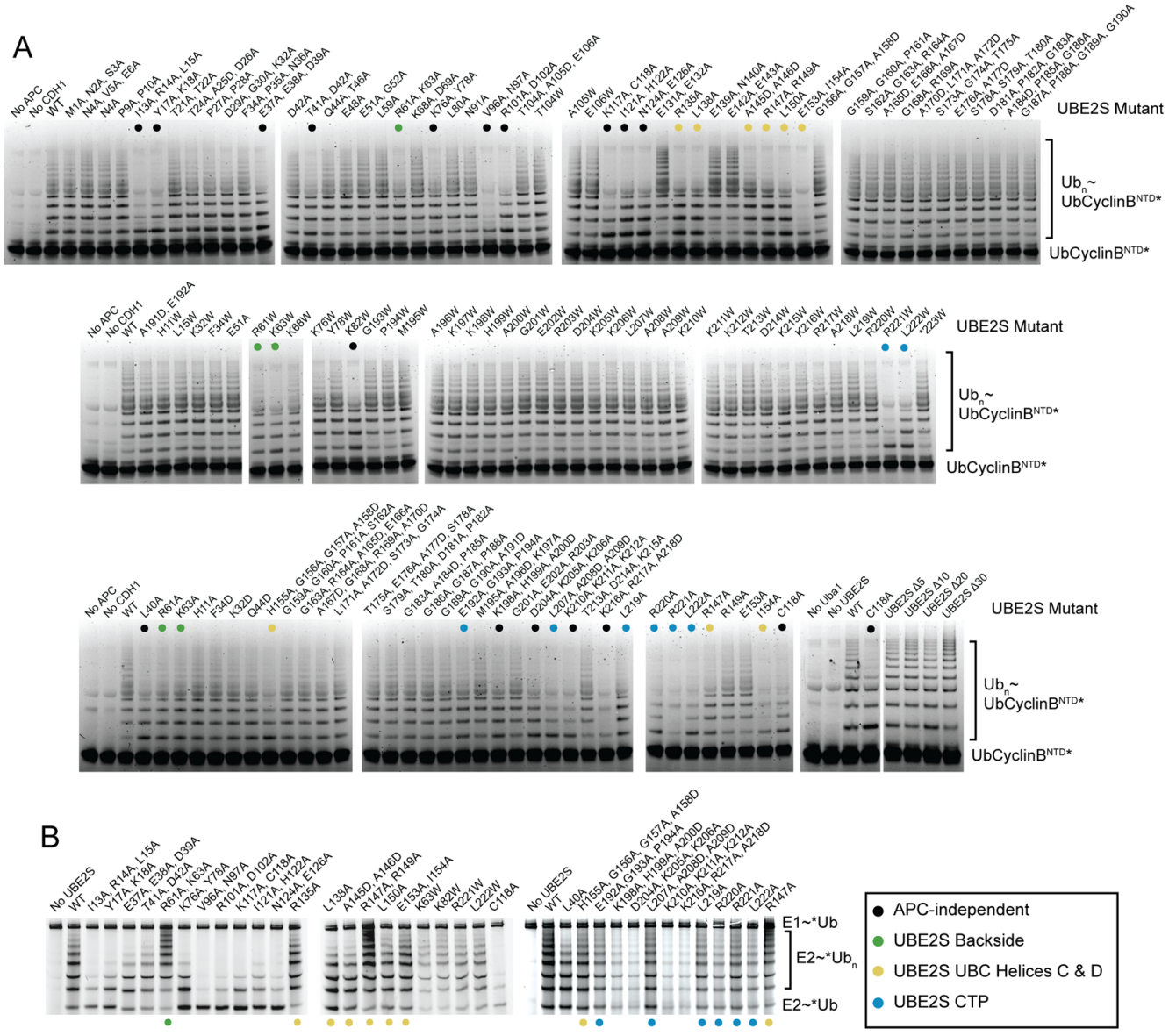
A
No APC
No CDH1
WT
M1A, N2A, S3A
N4A, V5A, E6A
N4A
P9A, P10A
I13A, R14A, L15A
Y17A, K18A
T21A, T22A
T24A, A25D, D26A
P27A, P28A
D29A, G30A, K32A
F34A, P35A, N36A
E37A, E38A, D39A
D42A
T41A, D42A
Q44A, T46A
E48A
E51A, G52A
L59A
R61A, K63A
K68A, D69A
K76A, Y78A
L80A
N91A
V96A, N97A
R101A, D102A
T104A, A105D, E106A
T104W
A105W
E106W
K117A, C118A
I121A, H122A
N124A, E126A
E131A, E132A
R135A
L138A
E139A, N140A
E142A, E143A
A145D, A146D
R147A, R149A
L150A
E153A, I154A
G156A, G157A, A158D
G159A, G160A, P161A
S162A, G163A, R164A
A165D, E166A, A167D
G168A, R169A
A170D, L171A, A172D
S173A, G174A, T175A
E176A, A177D
S178A, S179A, T180A
D181A, P182A, G183A
A184D, P185A, G186A
G187A, P186A, G189A, G190A
UBE2S Mutant
Ub$_n$~ UbCyclinB^{NTD*}
UbCyclinB^{NTD*}
No APC
No CDH1
WT
A191D, E192A
H11W
L15W
K32W
F34W
E51A
R61W
K63W
K68W
K76W
Y78W
K82W
G193W
P194W
M195W
A196W
K197W
K198W
H199W
A200W
G201W
E202W
R203W
D204W
K206W
L207W
A208W
A209W
K210W
K211W
K212W
T213W
D214W
K215W
K216W
R217W
A218W
L219W
R220W
R221W
L222W
*223W
UBE2S Mutant
Ub$_n$~ UbCyclinB^{NTD*}
UbCyclinB^{NTD*}
No APC
No CDH1
WT
L40A
R61A
K63A
H11A
F34D
K32D
Q44D
H155A, G156A, G157A, A158D
G159A, G160A, P161A, S162A
G163A, R164A, A165D, E166A
A167D, G168A, R169A, A170D
L171A, A172D, S173A, G174A
T175A, E176A, A177D, S178A
S179A, T180A, D181A, P182A
G183A, A184D, P185A
G186A, G187A, P188A
G189A, G190A, A191D
E192A, G193A, P194A
M195A, A196D, K197A
K198A, H199A, A200D
G201A, E202A, R203A
D204A, K205A, K206A
L207A, A208D, A209D
K210A, K211A, K212A
T213A, D214A, K215A
K216A, R217A, A218D
L219A
R220A
R221A
L222A
R147A
R149A
E153A
I154A
C118A
No Uba1
No UBE2S
WT
C118A
UBE2S Δ5
UBE2S Δ10
UBE2S Δ20
UBE2S Δ30
UBE2S Mutant
Ub$_n$~ UbCyclinB^{NTD*}
UbCyclinB^{NTD*}
B
No UBE2S
WT
I13A, R14A, L15A
Y17A, K18A
E37A, E38A, D39A
T41A, D42A
R61A, K63A
K76A, Y78A
V96A, N97A
R101A, D102A
K117A, C118A
I121A, H122A
N124A, E126A
R135A
L138A
A145D, A146D
R147A, R149A
L150A
E153A, I154A
K63W
K82W
R221W
L222W
C118A
No UBE2S
WT
L40A
H155A, G156A, G157A, A158D
E192A, G193A, P194A
K198A, H199A, A200D
D204A, K205A, K206A
L207A, A208D, A209D
K210A, K211A, K212A
K216A, R217A, A218D
L219A
R220A
R221A
L222A
R147A
E1~*Ub
E2~*Ub$_n$
E2~*Ub
APC-independent
UBE2S Backside
UBE2S UBC Helices C & D
UBE2S CTP

C

Data fitting for titrating UBE2S and variants in ubiquitination of Ub-CyclinB^{NTD*} by APC^{CDH1}

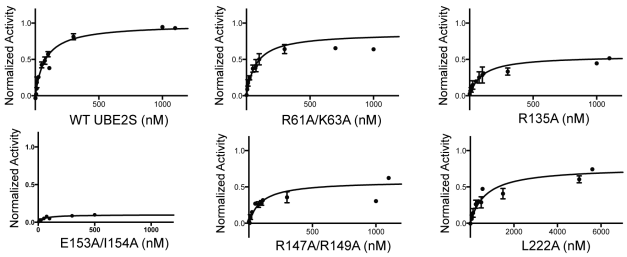

D

Data fitting for titrating UBE2S in di-Ub synthesis by APC variants

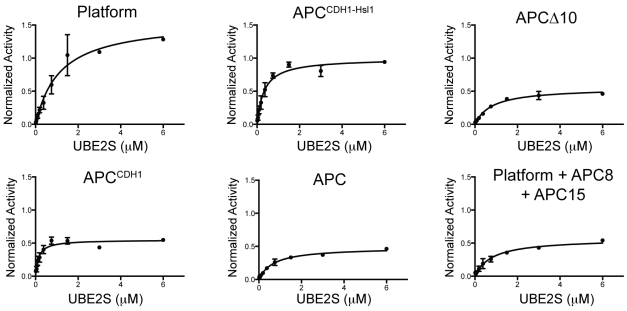

E

Data fitting for titrating Acceptor Ub in di-Ub synthesis by UBE2S and variants in the absence of APC

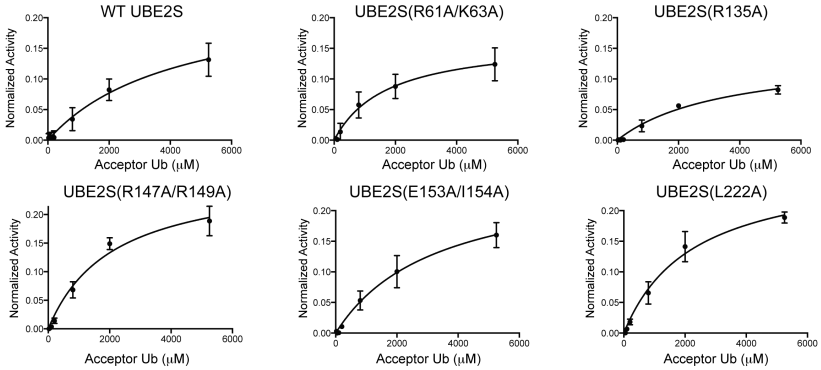

F

Data fitting for titrating Acceptor Ub in di-Ub synthesis by APC^{CDH1} with UBE2S and variants

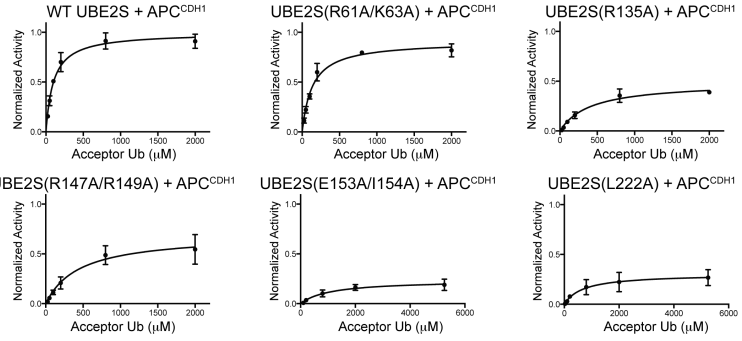

G

Data fitting for titrating UBE2S in ubiquitination of Ub-CyclinB^{NTD*} by APC^{CDH1} and APC11 RING mutants

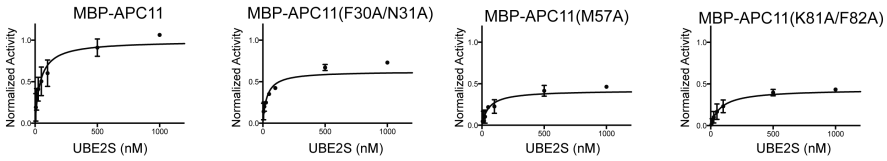

H

Data fitting for titrating Acceptor Ub in di-Ub synthesis by UBE2S and APC^{CDH1} and APC11 RING mutants

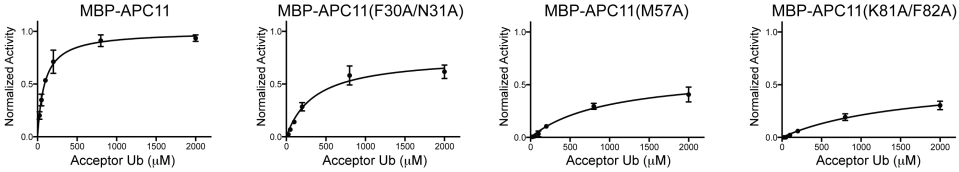

Figure S1. Representative fluorescence scans of raw SDS-PAGE data from UBE2S surface mutagenesis and fitting of kinetic data, related to Figure 1.

A, Data from 1st part of 2-part assay identifying UBE2S surfaces mediating APC-dependent ubiquitination. The need for an initiating E2 was bypassed by incorporating the priming Ub into a linear Ub-CyclinB^{NTD} fusion fluorescent substrate that is readily polyubiquitinated by APC^{CDH1}/UBE2S. Shown are representative fluorescence scans of raw SDS-PAGE data for Ub-CyclinB^{NTD}* ubiquitination by APC^{CDH1} and UBE2S (wild type and indicated mutant versions). Mutations causing decreased Ub-CyclinB^{NTD}* ubiquitination in presence of APC^{CDH1} are indicated with green, yellow and cyan dots, and structurally map to the backside of UBE2S' UBC domain, the C-terminal C and D helices of UBE2S' UBC domain, and the UBE2S C-terminal peptide (CTP), respectively. Black dots denote UBE2S mutants defective even in the absence of APC, identified in Fig. S1B. UBE2SΔ5, Δ10, Δ20, and Δ30 variants indicate that residues 181-186, 177-187, 167-187, and 160-190, respectively, were deleted from the UBE2S CTP.

B, 2nd part of 2-part assay identifying UBE2S surfaces mediating APC-dependent ubiquitination, filtering for APC-independent mutational defects by testing effects on UBE2S autoubiquitination. This reaction does not require APC, but as with APC-dependent ubiquitination, requires E1 charging and catalytic placement of the donor and acceptor Ub molecules. Shown are representative fluorescence scans of raw SDS-PAGE data monitoring autoubiquitination by fluorescent *Ub, with wild type UBE2S and the indicated mutant versions that were defective in the assay in Fig. S1A. Mutants specifically defective in APC-dependent ubiquitination shown above are indicated with green, yellow and cyan dots, based on their locations on the UBE2S structure.

C-H, Fitting of kinetic data. Error bars: SEM, n ≥ 3.
C, Titrations of UBE2S (wild type and indicated variants) in assays with fixed concentrations of APC^{CDH1} and Ub-CyclinB^{NTD}*.
D, Titrations of UBE2S (wild type and indicated variants) in di-Ub synthesis assays with fixed concentrations of APC variants and Ub*.
E, Titrations of acceptor Ub in di-Ub synthesis assays with fixed concentrations of UBE2S (wild type and indicated variants), without APC.
F, Titrations of acceptor Ub in di-Ub synthesis assays with fixed concentrations of APC^{CDH1} and UBE2S (wild type and indicated variants).
G, Titrations of UBE2S in assays monitoring ubiquitination of Ub-CyclinB^{NTD}*, with fixed concentrations of Ub-CyclinB^{NTD}* and APC^{CDH1} containing the indicated APC11 variants.
H, Titrations of acceptor Ub in di-Ub synthesis assays with fixed concentrations of APC^{CDH1} containing the indicated APC11 variants and UBE2S.

A

APC Subcomplex Name	APC Subunits	Figure
Platform Wild Type	APC1, APC4, APC5, APC2, APC11	2C, 2F, 2G
Platform MBP-11	APC1, APC4, APC5, APC2, His_6-MBP-APC11	2C
Platform MBP-11 ΔRING	APC1, APC4, APC5, APC2, His_6-MBP-APC11ΔRING	2C
APC 2/11	APC2 and APC11	2C, 2F, 3D
APC ΔAPC2 ΔAPC11	All APC Subunits except APC2 and APC11	2D
APC APC2 ΔCTD Δ11	All APC Subunits except APC11, and APC2 residues 1-548 only	2D
APC APC2 Δ4HB-CTD Δ11	All APC Subunits except APC11, and APC2 residues 1-445 only	2D
APC CFP-APC4ΔPropeller	All APC Subunits except APC4 residues 1-235 substituted with CFP	2D
Platform + APC8 + APC15	APC1, APC4, APC5, APC2, APC11, APC8, APC15	2G
APC ΔAPC10	All APC Subunits except APC10	2G
2/11 ΔRING	APC2 and APC11 ΔRING	3D
2 4HB-CTD/11	APC2 residues 446-822 and APC11	3D, 6C
2 4HB-CTD/MBP-11	APC2 residues 446-822 and His_6-MBP-APC11	3D
2 4HB-CTD/MBP-11ΔRING	APC2 residues 446-822 and His_6-MBP-APC11ΔRING	3D
APC MBP-APC11	All APC Subunits with His_6-MBP-APC11	4, 5A, 5B, 6A, 6B
2 4HB-CTD/11 ΔRING	APC2 residues 446-822 and APC11 ΔRING	6C
APC RING	APC11 residues 17-84	6D, 6E

B

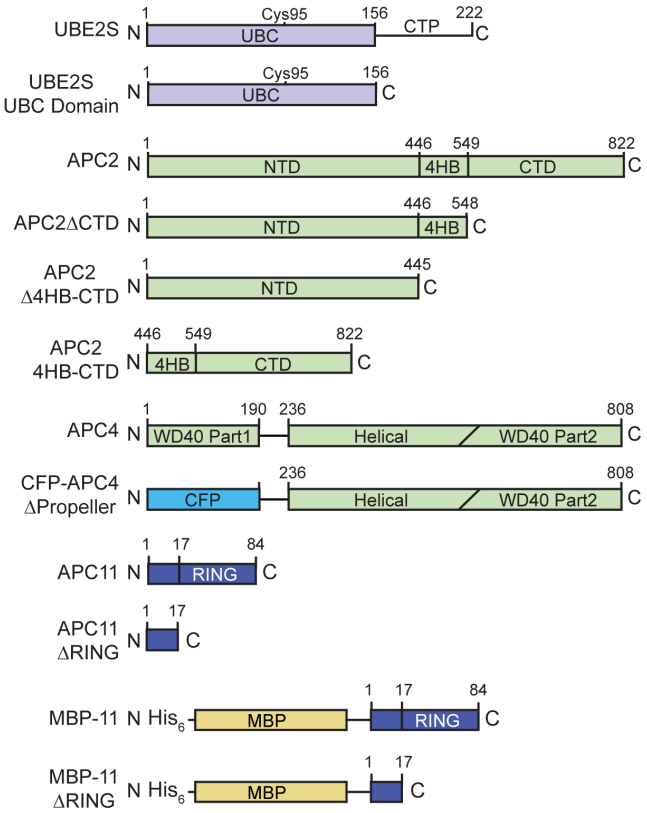

C

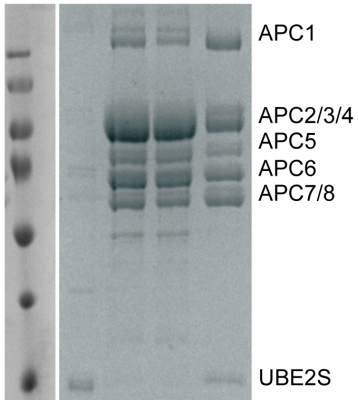

D

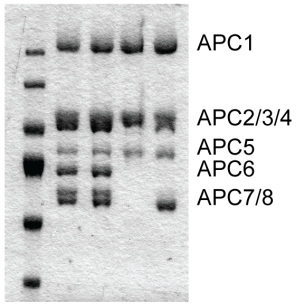

E

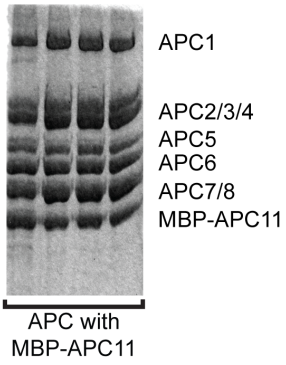

Figure S2. APC complexes and subcomplexes used in this study, related to Figure 2.

A, Table of APC complexes and subcomplexes, with names used in figures, their constituent APC subunits, and list of main figures in which they are used.

B, Schematic representation of primary structures of UBE2S, APC2, APC4, and various deletion mutants (not to scale). Domains of UBE2S: UBC – catalytic 'UBC' domain conserved among E2s; CTP – C-terminal peptide. Domains of APC2: NTD – N-terminal domain; 4HB – 4-helix bundle; CTD – C-terminal domain. Domains of APC4: WD40 – β-propeller; Helical – helical bundle domain. Domains of APC11: N-terminal domain followed by C-terminal RING domain; MBP – Maltose Binding Protein.

C, Affinity purification of recombinant APC bound to FLAG-tagged UBE2S used for EM. Coomassie-stained SDS-PAGE gel of the cryo-EM APC-UBE2S sample at different stages during the purification is shown. APC complexes used for scanning mutagenesis and immunoprecipitation analyses were purified based on affinity as shown, but those used in kinetic studies were further purified by ion exchange and gel filtration chromatography.

D, Coomassie-stained SDS-PAGE gel of purified APC subcomplexes used for kinetic studies in Fig. 2G.

E, Coomassie-stained SDS-PAGE gel of purified APC complexes containing His_6-MBP-APC11 RING mutants used for kinetic studies in Fig. 5B, 6A, 6B.

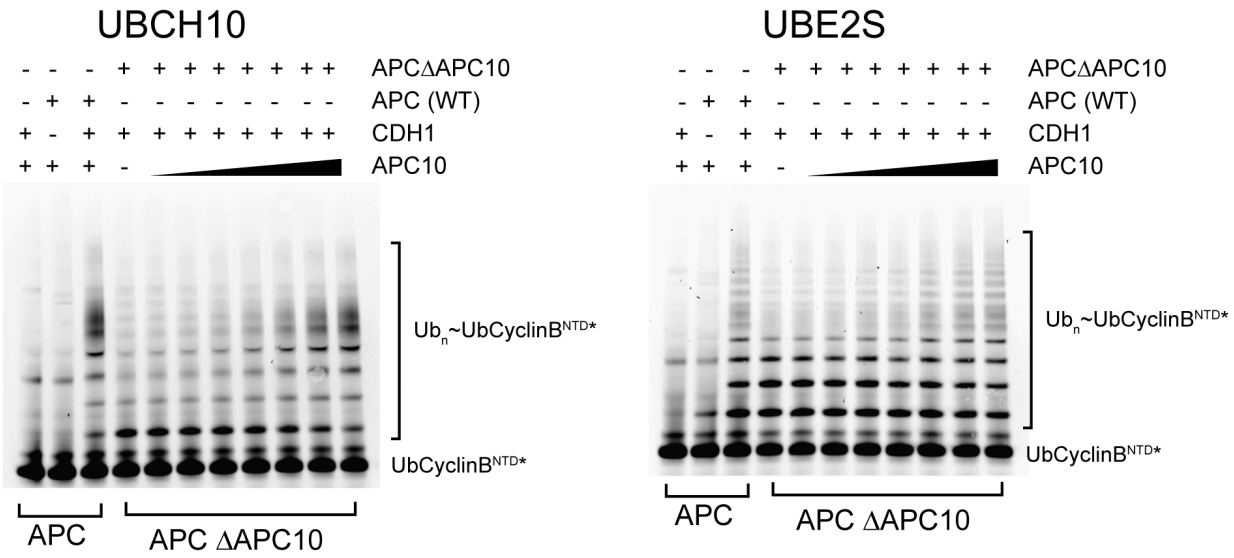

Figure S3. APC lacking APC10 is properly assembled, as addition of exogenous APC10 restores substrate-dependent ubiquitination activity, related to Figure 3. APC10 is required for processive APC^{CDH1}-dependent Ub-CyclinB^{NTD}* ubiquitination for both UBCH10 and UBE2S. Given a prior report that APC10 binds UBE2S (Sako et al., 2014), we also generated a version of APC lacking APC10, and validated its expected behavior toward Ub-CyclinB^{NTD}. Without APC10, which binds a substrate's D-box to enhance processivity of substrate ubiquitination, there was reduced generation of high molecular weight Ub conjugates on Ub-CyclinB^{NTD}*, but this was restored by adding bacterially expressed APC10 to reactions. Interestingly, however, deleting APC10 did not substantially influence either the K_m^{app} or V_{max}^{app} for UBE2S in di-Ub synthesis, which is independent of APC10's role in recruiting a substrate's D-box (Fig. 2G). Apparently, APC10 mediates its effects through means other than influencing the fundamental enzymatic function of forming Ub~Ub linkages.

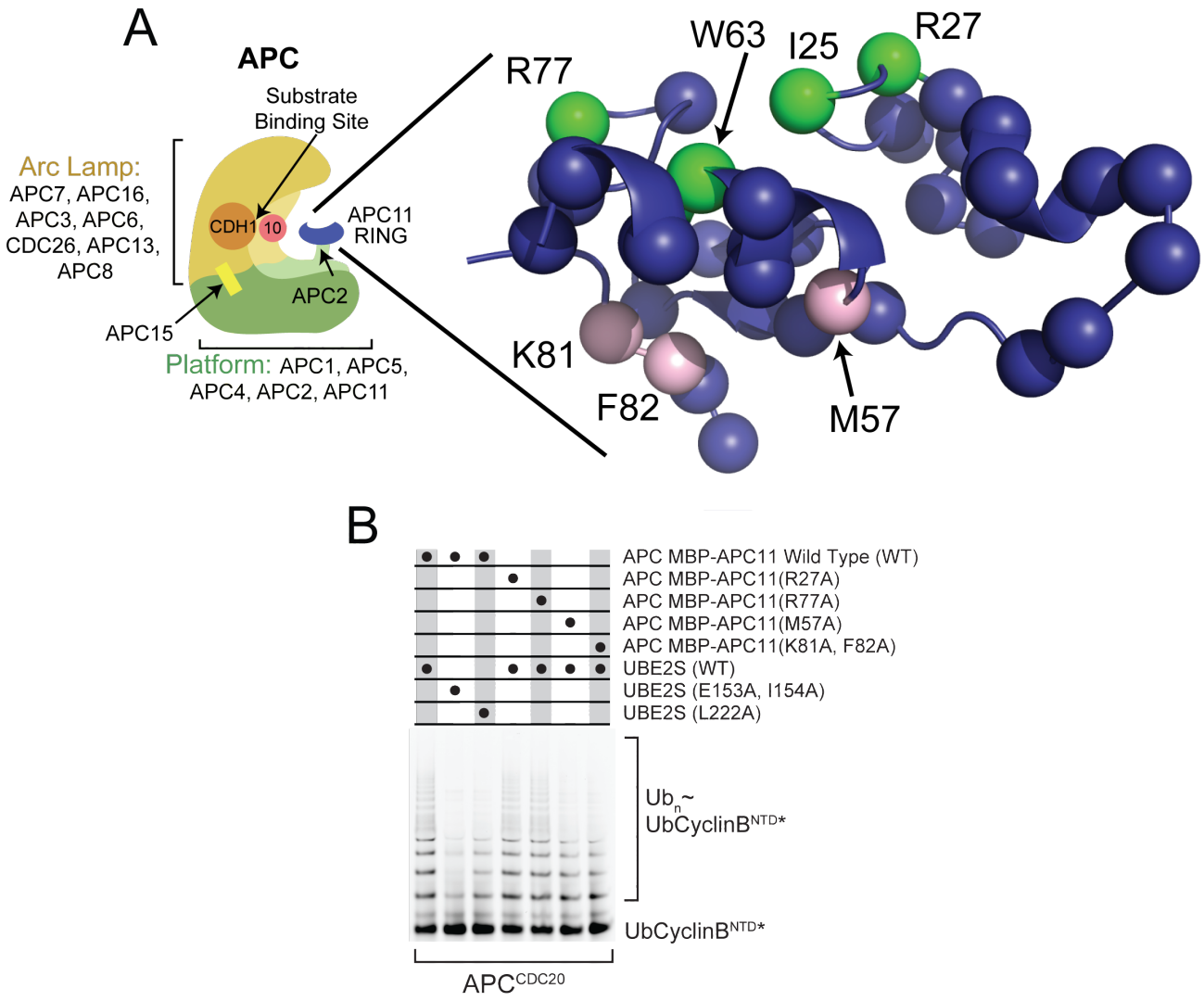

Figure S4. Alanine-scanning mutagenesis of APC11 RING domain within full APC complex, related to Figure 4.

A, Positions of Ala mutants are shown on the structure of the APC11 RING domain as spheres. APC complexes containing RING mutants were generated by coexpression of mutant versions of His_6-MBP-APC11 with all other APC subunits in insect cells. Canonical E2~Ub interacting residues for which mutations impaired ubiquitination by the Ub chain initiating E2s UBCH10 or UBCH5 are shown in green. Positions of mutations preferentially impairing ubiquitination by the Ub chain elongating E2, UBE2S, are shown in pink.

B, Mutations on UBE2S-specific RING surface, but not canonical E2~UB binding surface, impair Ub-CyclinB^{NTD*} polyubiquitination by APC^{CDC20}/UBE2S. Fluorescence scan of raw SDS-PAGE data.

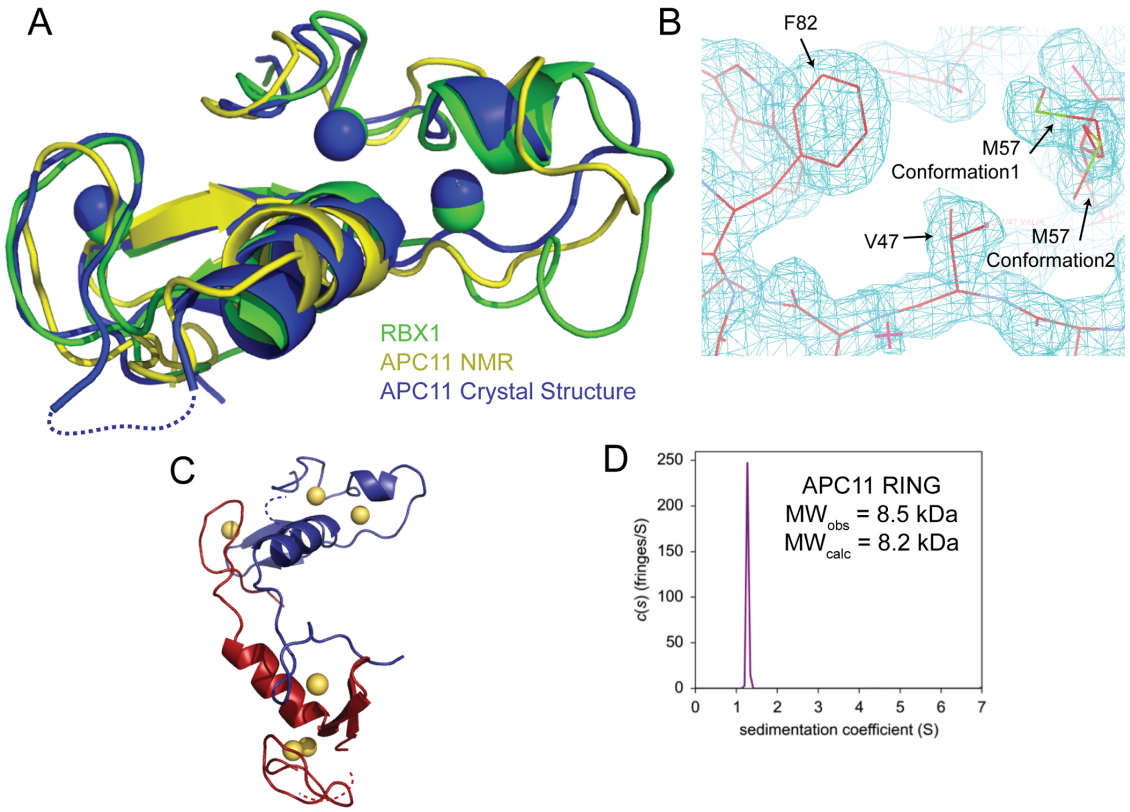

Figure S5. Structure determination of the human APC11 RING domain, related to Figure 5.

A, Crystal structure of APC11 RING domain in blue with zinc atoms as spheres, shown aligned with structure determined also by NMR (yellow) and the RING domain from RBX1 (green, from 1U6G.pdb, 0.94 RMSD (Goldenberg et al., 2004)). The crystal structure of the APC11 RING is a domain-swapped dimer. The domain swap occurs at the sequence Gln67-Gln68-Val69-Gln70-Gln71. For the figures of the APC11 RING domain structure, residues 21-68 are shown from one protomer, and 70-84 from the opposite protomer in the domain-swapped dimer to generate a single composite RING domain as shown here.

B, Representative electron density for the APC11 RING domain, shown over the surface involved in acceptor Ub recruitment in APC-UBE2S-mediated di-Ub synthesis. The side-chain of Met57 is modeled in two alternative conformations.

C, One domain swapped-dimer from the crystal structure of the APC11 RING domain. Two of four protomers in the asymmetric unit shown in blue and red, respectively, with zinc ions as yellow spheres.

D, Analytical ultracentrifugation data reveals the isolated APC11 RING domain protein samples used in the studies herein is predominantly monomeric in solution. The sedimentation velocity profiles (fringe displacement) were fitted to a continuous sedimentation coefficient distribution model c(s). The experiments were conducted in 25 mM Tris pH 7.6, 100 mM NaCl and 1 mM DTT buffer at 20 °C and at a rotor speed of 50,000 rpm. The measured molecular weight of 8.5 kDa corresponds well with the calculated mass of 8.2 kDa for a monomer.

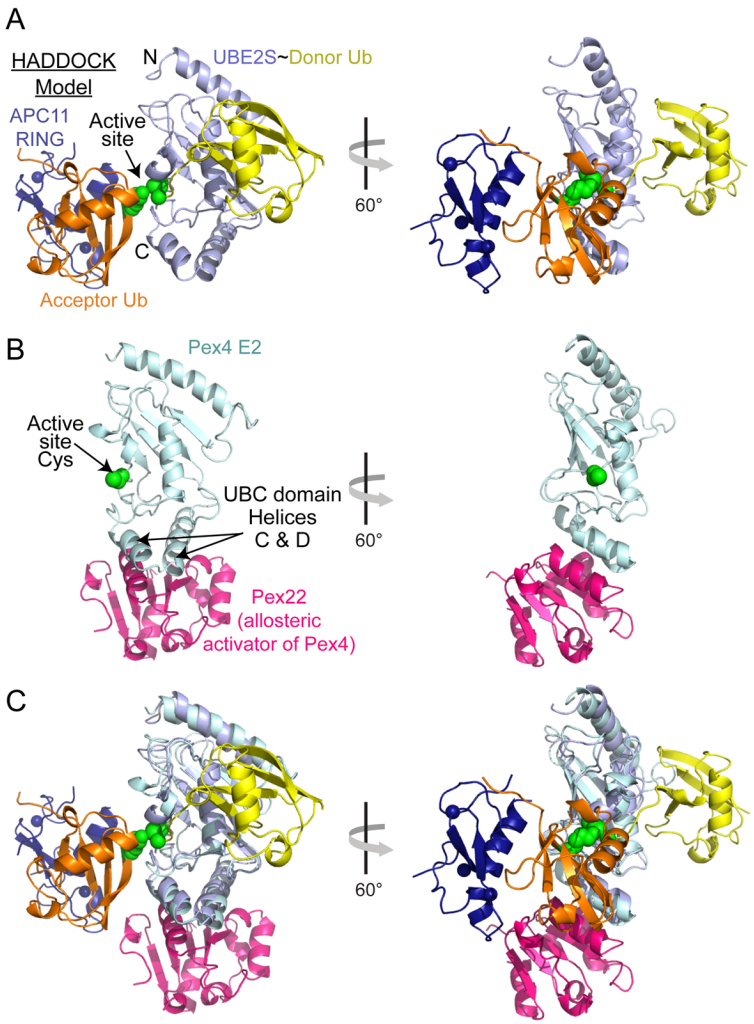

Figure S6. Structural modeling providing insights into distinctive RING-dependent APC activation of UBE2S-mediated Ub chain elongation, related to Figure 7.

A, Model of a ^{Donor}Ub~UBE2S-^{Acceptor}Ub-APC11 RING intermediate. Results of HADDOCK docking of APC11 RING (blue) with the acceptor Ub (orange) is modeled on the structure of the UBE2S UBC domain shown in slate (Sheng et al., 2012), according to (Wickliffe et al., 2011). The donor Ub (yellow) was modeled by aligning the structure of the UBE2S UBC domain and a structure of a ^{Donor}Ub~E2 complex (Plechanovova et al., 2012).

B, Structure of the *S. cerevisiae* E2 Pex4 (pale cyan) in complex with its activator, Pex22 (magenta), involved in a peroxisomal ubiquitination pathway (Williams et al., 2012). Notably, Pex22 interactions with Pex4 helices C and D allosterically activate Ub ligation through poorly defined mechanisms.

C, Compatibility and proximity of multiple modes of APC activation of Ub chain elongation with UBE2S. From APC, the APC11 RING helps recruit the acceptor Ub, and the APC2-APC4 region activates the UBE2S helix D. The interactions are compatible and spatially near each other as shown by superimposing the model in A for APC RING-dependent recruitment of the acceptor Ub to a UBE2S~Ub intermediate, and the UBC domain activation from the peroxisomal pathway in B.

Supplemental Experimental Procedures

Purification of proteins for enzyme assays, coimmunoprecipitation experiments, NMR, and crystallography

Recombinant APC and its subcomplexes were expressed in a baculovirus expression system similar to that described previously (Frye et al., 2013), although the only affinity tag was a twin-Strep tag at the C-terminus of APC4 similar to that used in recent structural studies (Chang et al., 2014). For all experiments other than EM and the experiments shown in Fig. 5A, APC, Platform, and other subcomplexes were purified with a 3-step scheme: Affinity purification with Strep-Tactin Sepharose (IBA Lifesciences) and elution with desthiobiotin, anion exchange, and size exclusion chromatography in a final buffer of 20 mM HEPES pH 8.0, 200 mM NaCl, 1 mM DTT. For the broad mutagenesis screen of RING domain mutants shown in Fig. 5A, APC complexes containing His_6-MBP-APC11 were purified by affinity chromatography based on the tag on APC4, with Strep-Tactin Sepharose, but APC incorporating RING mutants studied in Fig. 4, 5B, 6A, 6B, S1, and S4B were all purified using the 3-step scheme.

Wild type and mutant versions of UBE2S were expressed in BL21(DE3) Codon Plus (RIL) cells, from a modified pRSF-1b vector with a His_6-TEV protease site-FLAG-HRV13 3C protease site-fused to the N-terminus. For the Ala and Trp scanning mutagenesis described in Fig. 1D and S1, these were purified by nickel affinity chromatography, cleaved off the beads with HRV13 3C protease protease, and purified by cation exchange using gravity columns and bump elution with 20 mM TRIS pH 7.6, 400 mM NaCl, 1mM DTT. Concentrations of mutants were all normalized with this elution buffer prior to use, in order to ensure equal buffer and salt concentrations in assays. UBE2S and mutants used for kinetic and other follow-up enzyme assays (Fig. 1E, 2F-G, 3A-D, 4, 5A-B, 6A-B, 6F, S1C-H, S3 and S4B) were purified by nickel affinity chromatography, eluted, cleaved in solution by HRV13 3C protease, and further purified by cation exchange chromatography and size exclusion chromatography into a final buffer of 20 mM HEPES pH 8.0, 200 mM NaCl, 1 mM DTT. UBE2S and mutants used for FLAG immunoprecipitations in Fig. 2B, C, and D were purified by nickel affinity chromatography, eluted, and further purified by cation exchange using gravity columns and bump elution with 20 mM TRIS pH 7.6, 400 mM NaCl, 1mM DTT.

N-terminal 3xMYC-His_6-CDH1, 3xMYC-His_6-CDC20, UBCH10-His_6, and human E1 were purified as described previously (Frye et al., 2013; Uzunova et al., 2012). All other proteins were expressed in the BL21-CodonPlus(DE3)-RIL strain of *E. coli*, except the APC11 RING (residues 17-84) that was expressed in BL21-GOLD(DE3). APC11 RING domain for NMR was expressed as described previously for $EMI1^{ZT}$ in (Frye et al., 2013). Free APC10 and APC11 were expressed as a TEV protease cleavable N-terminal GST fusions, purified by glutathione-affinity chromatography and treated with TEV protease to cleave off the GST-tag. APC10 was further purified by cation exchange and size exclusion chromatography. APC11 was further purified with size exclusion chromatography. The $CyclinB^{NTD}$ (residues 1-95) and Ub-$CyclinB^{NTD}$ substrates were expressed as N-terminal GST fusions with a C-terminal Cys-His_6 tag and purified by nickel affinity chromatography, treated with TEV to remove tags, and polished with size exclusion chromatography. Untagged Ub was purified by an acetic acid precipitation step of unwanted bacterial proteins followed by cation exchange and size exclusion chromatography.

The Ub used as donor in assays in Figs. 1E, 2F-G, 3C-D, 4, 5A-B, 6A, S1C-D, S1G, S3, and S4B, and as acceptor in Figs. 3A-B, 6B, S1E-F, and S1H was purified largely as described previously (Pickart and Raasi, 2005). The fluorescent donor Ub (*Ub) for experiments in Figs. 3A-B, 6B, S1E-F, and S1H and the fluorescent acceptor Ub (Ub*) for experiments in Figs. 2F-G, 3D, and S1D were expressed as a N-terminal GST

fusion and purified by glutathione-affinity chromatography, TEV-mediated proteolytic cleavage of the GST-tag, and size exclusion chromatography. The fluorescent donor and acceptor ubiquitin contained a single cysteine at either position -1 or 77 (G75S:G76S:C77), respectively, for fluorescein-5-maleimide labeling described below. The Ub variants screened for ability to serve as acceptor Ub in Fig. 6F were expressed as Ub (1-74)-Ala-His_6 fusions and purified by nickel affinity chromatography, with buffer matching and removal of imidazole by desalting with PD-10 columns (GE Healthcare: Life Sciences) into 50 mM HEPES pH 7.0, 150 mM NaCl.

APC-UBE2S complex purification for cryo Electron Microscopy

APC was initially purified by incubation with Strep-Tactin Sepharose. After washing the Strep-Tactin resin, 5 µM His_6-TEV-FLAG-PreScission-UBE2S was incubated with resin-bound APC for 1 hour. The resin was washed with 50 mM HEPES pH 8.0, 150 mM NaCl, 2.5% glycerol, 0.05% Tween 20, and the APC-UBE2S complex was eluted with wash buffer supplemented with 2.5 mM desthiobiotin (Sigma). The eluate was then incubated with Anti-FLAG M2 affinity gel (Sigma) for 1 hour, washed with 50 mM HEPES pH 8.0, 150 mM NaCl, 2.5% glycerol, 0.05% Tween 20, and eluted with this wash buffer supplemented with 0.1 mg/ml FLAG peptide. The equivalent of 250 µg of APC-UBE2S was further processed through GraFix (Kastner et al., 2008).

Cryo Electron Microscopy

For cryo-EM, the buffer of GraFix-purified fractions was exchanged for 50 mM HEPES pH 8.0, 150 mM NaCl, 2 mM $MgCl_2$ by desalting (Zeba spin column, Pierce). Particles were adsorbed on carbon film for 1 minute and then mounted on an EM copper grid covered with a perforated carbon film. Specimens were blotted and vitrified (Vitrobot, FEI Company). Images were recorded at a magnification of 74,000x (2 Å/pixel) under cryogenic conditions in a C_s corrected Titan Krios (FEI Company) electron microscope on a Falcon II direct electron detector (FEI Company). The image dataset was corrected for the CTF (Sander et al., 2003) and particles were iteratively aligned applying resampling to polar coordinates (Sander et al., 2003) and multivariate statistical classification (van Heel, 1984). By computational sorting we found populations of APC particles with UBE2S bound in two distinct conformations and a population where UBE2S was lacking. Both APC/C-UBE2S 3D structures were calculated from ~20,000 particle images and a resolution of 13Å and 23Å were obtained (as judged by the FSC 0.143 criterion, calculated from two independently processed half datasets). Figures were generated using Chimera (Pettersen et al., 2004).

Enzyme Assays

The APC/C ubiquitination assays were performed as previously described (Frye et al., 2013), with some differences. The $CyclinB^{NTD}$ and Ub-$CyclinB^{NTD}$ substrates and fluorescent ubiquitins were labeled using fluorescein-5-maleimide (Pierce). Single cysteine proteins were first reduced with 20 mM DTT and desalted twice with Nap5 columns (GE Healthcare: Life Sciences) into 50 mM HEPES pH 7.0, 150 NaCl. The fluorescein-5-maleimide, dissolved in DMSO, was then added in 5-fold molar excess to the protein solution. The reaction was incubated at room temperature for ~2 hours. The reaction was then quenched with 10 mM DTT and subsequently desalted using a PD10 column into 50 mM HEPES pH 7.0, 150 NaCl, 10 mM DTT. Size exclusion chromatography was used to further remove the free fluorescent label using 20 mM HEPES pH 8.0, 200 mM NaCl, 1 mM DTT.

The assays were performed in the same buffer used for gel filtration of APC (20 mM HEPES pH 8.0, 200 mM NaCl, 1 mM DTT). Proteins were mixed on ice containing

APC, ubiquitination substrate (Ub, Ub*, *Ub, CyclinB^{NTD}* or Ub-CyclinB^{NTD}*) in 5 mM $MgCl_2$, 5mM ATP, 0.25 mg/mL BSA, with 1 μM CDH1 and 0.1 μM E1 and E2. The reaction mixtures were then equilibrated to room temperature before the reactions were initiated by adding 0.2 mM donor Ub. For all kinetic analyses, product bands were quantitated based on a fluorescein label on *Ub, Ub*, or Ub-CyclinB^{NTD}* using a Typhoon FLA 9500 PhosporImager. For APC-dependent Ub-CyclinB^{NTD}* reactions, APC-independent products were subtracted as background. For APC-independent reactions, products from a negative control reaction that did not contain the ^{Acceptor}Ub were subtracted as background.

Kinetic experiments to determine the apparent K_m (K_m^{app}) and apparent V_{max} (V_{max}^{app}) values were determined by fitting the initial velocities to the hyperbolic Michaelis-Menten, $v = V_{max}^{app}[X]/(K_m^{app} + [X])$, equation, where X is either the UBE2S or ^{Acceptor}Ub concentration, using GraphPad Prism 6 software. Single time points were taken under conditions that satisfy initial velocity regimes. In summary, a time course was monitored at both the minimum and maximum point of each titration to ensure a single time point could be taken where the substrate or UBE2S~Ub depletion are minimal and product formation remained linear. The activity for each quantitative assay was normalized to the V_{max}^{app} of wild-type UBE2S with either APC^{CDH1} or APC$^{CDH1\text{-}Hsl1}$ depending on the experiment described.

To determine the K_m^{app} and V_{max}^{app} values for UBE2S in assays monitoring Ub-CyclinB^{NTD}* ubiquitination or di-Ub synthesis using Ub* as the substrate, the concentrations were 10 nM or 30 nM APC variant, and 0.5 μM Ub-CyclinB^{NTD}* or 4 μM Ub*. Reactions were quenched after 10 min or 20 min, depending on the components. The assays monitoring Ub transfer to an acceptor Ub* were performed in similar conditions as assays for Ub-CyclinB^{NTD}* ubiquitination assays, except the acceptor substrate was Ub-fluorescein (G75S:G76S:C77). This C-terminal Cys is fluorescently labeled and prevents the Ub-fluorescein from conjugating to either the E1 or E2. For the assays monitoring ubiquitination of Ub-CyclinB^{NTD}*, the data were normalized to the V_{max}^{app} of wild type UBE2S-APC^{CDH1}. For the assays monitoring Ub transfer to Ub*, the data were normalized to the V_{max}^{app} of wild type UBE2S-APC$^{CDH1\text{-}Hsl1}$.

Qualitative assays probing the function of UBE2S were performed as described above except with concentrations of 14 nM APC, 0.25 μM UBE2S, 0.5 μM Ub-CyclinB^{NTD}* were used (Fig. 1D and S1A). These reactions were quenched at 10 min. The UBE2S autoubiquitination assays (Fig. 1D and S1B) were carried out similarly except (1) the only Ub source was fluorescein-labeled wild type *Ub used at 4 μM concentration; (2) APC^{CDH1} and Ub-CyclinB^{NTD}* were absent; and (3) the reactions were quenched after 60 min.

Qualitative assays probing the function of His_6-MBP-APC11 RING domain in the context of APC (Fig. 5A) were performed as described above except concentrations of 50 nM APC, 1 μM CDH1, 0.2 μM UBCH5B, UBCH10 or UBE2S, 0.2 μM CyclinB^{NTD} or Ub-CyclinB^{NTD}* were used. These reactions were quenched at 15 min. Qualitative assays in Figs. 4, 5B, and S3 were performed similarly, except the APC concentration is 30 nM APC and in Fig S4B, 0.6 μM CDC20 was used instead of CDH1.

To determine the K_m^{app} and V_{max}^{app} values for the acceptor Ub, 20 μM of the fluorescein-labeled wild-type *Ub was first loaded onto 10 μM E1 in the presence of 5 mM MgCl2 and 5 mM ATP for 10 min at room temperature. Formation of the E1~*Ub intermediate was quenched with 25 mM EDTA and two passes over desalting columns (Zeba spin column, Pierce) to remove and/or chelate the MgATP to prevent reloading of the E1. The E1~*Ub was then diluted into a second independent mixture (final concentration 2 μM E1~*Ub) that contained unlabeled Ub, BSA, 0.2 μM UBE2S and 0.1 μM APC^{CDH1}, and ubiquitination reactions were then carried out for 3 min. The data were normalized to the V_{max}^{app} of wild type UBE2S-APC^{CDH1}.

For qualitative assays probing the function of the acceptor Ub mutants (Fig. 6F), the E1 charging reaction was started with addition of E1, Ub and MgATP. Formation of the E1~Ub intermediate was quenched by adding EDTA and subsequent desalting. The reaction was then added to a mixture containing UBE2S and Ub or UBE2S, APC^{CDH1}, and Ub. The Ub (1-74)-Ala-His_6 fusion variants were screened in the APC^{CDH1}-independent and APC^{CDH1}-dependent assays at concentrations similar to the apparent K_m^{app} values for wild type acceptor Ub as follows: 0.1 μM APC^{CDH1}, 2 μM UBE2S, and 0.1 mM Ub for 5 min in the APC^{CDH1}-dependent assay and 20 μM UBE2S and 1 mM Ub for 15 min in the APC^{CDH1}-independent assay. The UBE2S and Ub concentrations used in APC-dependent and APC-independent assays differ to compensate for the different K_m^{app} and V_{max}^{app} values in the presence or absence of APC^{CDH1}.

BPA-UBE2S Protein Expression and Purification

Amber codons and deletion of CTP "LRRL" residues of UBE2S mutants were introduced into pGEX modified with GST-TEV-FLAG-PreScission. These various amber codon-containing UBE2S constructs were co-transformed into BL21(DE3) with pEVOL-*pBpF*, a plasmid that encodes aaRS for *p*-Benzoyl-L-Phenylalanine (BPA) and modified tRNA that repurposes the TAG codon for ribosomal incorporation of BPA (Addgene plasmid 31190) (Young et al., 2010). Proteins were expressed overnight at 23° in auto-induction media and induced simultaneously with 0.02% Arabinose (Sigma), 0.6 mM IPTG, and 0.2 mM BPA dissolved immediately prior to use at 50 mM in 0.7 M NaOH. BPA-UBE2S proteins were purified by glutathione-affinity and cation exchange chromatography. Incorporation of BPA was verified by Intact Mass Spectrometry for the BPA-UBE2S variants (Hartwell Center, St. Jude Proteomics/Mass Spectrometry Facility). *p*-Benzoyl-L-Phenylalanine (BPA) was purchased from Bachem.

Photocrosslinking BPA-UBE2S with APC

Photocrosslinking experiments were performed on ice by mixing BPA-UBE2S with APC-His_6-MBP-APC11 and 3xMYC-His_6-CDH1 at 1 μM. Following a 60-minute exposure to 365nm UV light (Bulb ID: 34-0009-01) proteins were separated by 15% (FLAG-UBE2S blot) or 8% (APC subunit blots) SDS-PAGE. The following commercial antibodies were used for detection in crosslinking studies by western blotting using standard methods: APC1 (SC-20983, SCBT), APC2 (12301, Cell Signaling Technology), APC4 (SC-21414, SCBT), APC11 (14090, Cell Signaling Technology), Strep-Tag II (Ab76949, Abcam), FLAG (F1804, Sigma-Aldrich), and c-MYC (SC-40, SCBT). Polyclonal APC5 antibodies were generated at Gramsch Laboratories against a synthetic peptide (ELTSRDEGERKMEKEEL).

X-Ray Crystallography

APC 11 RING domain (residues 17-84) was purified in 25 mM TRIS pH 7.6, 100 mM NaCl, 1 mM DTT. Crystals were grown with the hanging drop vapor diffusion method in 16% PEG 3350, 0.2 M $NaNO_3$, 0.1 M BIS-TRIS Propane pH 6.5 and set at room temperature with 30 mg/mL APC11 RING domain. The mother liquor including 40% PEG 3350 was used as a cryoprotectant. The data were collected at NECAT ID-24C at the Zn peak energy. The data were integrated and scaled using the NECAT RAPD software (https://rapd.nec.aps.anl.gov/rapd). The initial phasing electron density was obtained with zinc SAD using SHELX (Sheldrick, 2008). Model construction and refinement were done in Coot (Emsley and Cowtan, 2004; Emsley et al., 2010) and Phenix (Adams et al., 2010).

NMR Spectroscopy

NMR samples were purified in 20 mM Hepes pH 7.0, 100 mM NaCl, 10 mM DTT dissolved in 90% H_2O/10% D_2O buffer. All the titration data were collected as 2D [^{15}N, ^{1}H] TROSY spectra at 298K with a Bruker 800 MHz spectrometer equipped with a ^{1}H and ^{13}C detector, TCI triple resonance cryogenic probe on ^{15}N-labeled samples. The assays monitoring chemical shift perturbations upon adding $APC2^{4HB\text{-}CTD}$ /APC11±RING to ^{15}N-labeled Ub were performed at concentrations of 0.24 mM and 0.1 mM, respectively. An APC11 RING titration ranging from 0.1 - 1.3 mM was added to 0.2 mM ^{15}N-labeled Ub. An Ub titration ranging from 0.2 - 3 mM was added to 0.1 mM ^{15}N-labeled APC11 RING. RING domain assignment experiments were carried out on ^{15}N, ^{13}C labeled APC11 RING at 500 µM concentration. APC11 RING domain backbone resonance 3D NMR experiments were measured on a Bruker 600 MHz spectrometer equipped with a ^{1}H and ^{13}C detect, TCI triple resonance cryogenic probe using standard Bruker pulse programs. ^{1}H, ^{13}C, and ^{15}N backbone resonances were assigned using standard triple resonance experiments, such as HNCACB, CBCA(CO)NH, HNCO and HN(CA)CO. Side chain assignments were carried out using ^{15}N-resolved TOCSY, ^{13}C-resolved H(C)CH TOCSY and (H)CCH TOCSY experiments. Aromatic side chains were assigned using the 13C-resolved aromatic NOESY spectra along with the TOCSY. All the ^{1}H chemical shifts were referenced with respect to DSS measured in the same buffer, while the ^{13}C and ^{15}N chemical shifts were referenced indirectly with respect to the DSS shift. All of the spectra were processed using TopSpin software and analyzed using the computer-aided resonance software, CARA (Keller, 2004). Ubiquitin assignments were taken from BMRB entry 15410 (Wong et al., 2008). The chemical shift perturbations were calculated using, $CSP(ppm) = [(\Delta\delta H)^2 + (1/2)(\Delta\delta N)^2]^{0.5}$, where $\Delta\delta H$ and $\Delta\delta N$ represents the chemical shift difference between the free and complex for ^{1}H and ^{15}N resonances respectively.

Structures were determined using a combination of manually assigned NOEs and automatic NOE assignment using the program CYANA (Guntert et al., 1997). Approximately 872 meaningful distance restraints, 32 angle restraints derived from CA, CB shifts using program TALOS+(Shen et al., 2009), 12 zinc ion distances and 18 hydrogen bond restraints based on exchange cross peaks with water in the ^{15}N-NOESY spectrum, were used in the structure calculation of APC11 RING. Seven iterations of refinement of 100 structures per cycle were completed, after proper distance calibrations. After the initial fold of the protein was determined, a CYANA amino acid library using a modified zinc-ligated cysteine residue was used to incorporate the three zinc ions into the structures. Parameters used in the structure calculation are given in Table 2.

Analytical Ultracentrifugation

Sedimentation velocity experiments were conducted in a ProteomeLab XL-I analytical ultracentrifuge (Beckman Coulter, Indianapolis, IN) following standard protocols unless mentioned otherwise (Zhao et al., 2013a). The sample in a buffer containing 25 mM Tris pH 7.6, 100 mM NaCl, and 1 mM DTT was loaded into a cell assembly comprised of a double sector charcoal-filled centerpiece with a 12 mm path length and sapphire windows. The density and viscosity of the ultracentrifugation buffer at 20 °C were measured with a DMA 5000M density meter and an AMVn viscometer (both Anton Paar, Graz, Austria) respectively. The cell assembly, containing identical sample and reference buffer volumes of 400 µL, was placed in a rotor and temperature equilibrated at 20 °C at rest for 2 hours before it was accelerated from 0 to 50,000 rpm. Rayleigh interference optical data were collected at 1-minute intervals for 12 hours. The velocity data were modeled with diffusion-deconvoluted sedimentation coefficient distributions c(s) in SEDFIT (https://sedfitsedphat.nibib.nih.gov/software/default.aspx), using algebraic noise decomposition and with signal-average frictional ratio and meniscus position refined with

non-linear regression. The s-value was corrected for time, temperature and radial position and finite acceleration of the rotor was accounted for in the evaluation of Lamm equation solutions (Ghirlando et al., 2014; Zhao et al., 2013b). Maximum entropy regularization was applied at a confidence level of P-0.68.

Computational modeling APC11 RING-^{Acceptor}Ub interactions

We used Haddock 2.1 (de Vries et al., 2007; Dominguez et al., 2003) for constructing the RING-^{Acceptor}Ub complex. The HADDOCK run produced an ensemble of 200 structures, which were clustered by applying backbone root-mean-square deviation (rmsd) cut-off of 7.5 angstrom after two-step HADDOCK simulations. To model the RING-^{Acceptor}Ub complex, the crystal structure of the APC11 RING domain was docked to a single Ub molecule. The binding interface of the RING domain and acceptor Ub was defined from NMR chemical shift perturbation data by mutual titrations of the RING domain and ubiquitin. Two loops of the acceptor Ub, residues 8-10 and 72-76, were set as flexible residues in explicit solvent refinement stage, to allow the system to fully explore more favorable conformations of these regions while maintaining the overall complex architecture. Interactions of side chains with three zinc ions were kept during simulations by adding additional unambiguous distance restraints. The simulation generated 2 clusters. The cluster 1 contains 87% of all modeled structures with better average binding affinity within the top ranked four structures as shown below:

The calculated binding free energies of top ranked models in the two HADDOCK clusters.

	Number of Structures[b]	**E_{tot}[c] (k_{cal}/mol)**	**E_{vdw}[d] (k_{cal}/mol)**	**E_{elec}[e] (k_{cal}/mol)**
Cluster 1 (top 4)[a]	164	-3.37 +/- 0.22	-0.83 +/- 0.30	-2.54 +/- 0.33
Cluster 2 (top 4)	26	-0.63 +/- 0.63	-0.50 +/- 0.49	-0.13 +/- 0.67

[a] The top four models with best binding free energies from each cluster were used to determine the average binding free energies and standard deviations .

[b] Indicates that the number of structures in each cluster which share similar conformations with backbone rmsds within 7.5 angstroms.

[c] E_{tot} indicates the total binding free energy.

[d] E_{vdw} indicates the average van der waals interaction energy.

[e] E_{elec} indicates the average electrostatic interaction energy.

SUPPLEMENTAL REFERENCES

Adams, P.D., Afonine, P.V., Bunkoczi, G., Chen, V.B., Davis, I.W., Echols, N., Headd, J.J., Hung, L.W., Kapral, G.J., Grosse-Kunstleve, R.W.*, et al.* (2010). PHENIX: a comprehensive Python-based system for macromolecular structure solution. Acta crystallographica *66*, 213-221.

Chang, L., Zhang, Z., Yang, J., McLaughlin, S.H., and Barford, D. (2014). Molecular architecture and mechanism of the anaphase-promoting complex. Nature.

de Vries, S.J., van Dijk, A.D., Krzeminski, M., van Dijk, M., Thureau, A., Hsu, V., Wassenaar, T., and Bonvin, A.M. (2007). HADDOCK versus HADDOCK: new features and performance of HADDOCK2.0 on the CAPRI targets. Proteins *69*, 726-733.

Dominguez, C., Boelens, R., and Bonvin, A.M. (2003). HADDOCK: a protein-protein docking approach based on biochemical or biophysical information. Journal of the American Chemical Society *125*, 1731-1737.

Emsley, P., and Cowtan, K. (2004). Coot: model-building tools for molecular graphics. Acta crystallographica *60*, 2126-2132.

Emsley, P., Lohkamp, B., Scott, W.G., and Cowtan, K. (2010). Features and development of Coot. Acta crystallographica *66*, 486-501.

Frye, J.J., Brown, N.G., Petzold, G., Watson, E.R., Grace, C.R., Nourse, A., Jarvis, M.A., Kriwacki, R.W., Peters, J.M., Stark, H.*, et al.* (2013). Electron microscopy structure of human APC/C(CDH1)-EMI1 reveals multimodal mechanism of E3 ligase shutdown. Nature structural & molecular biology *20*, 827-835.

Ghirlando, R., Zhao, H., Balbo, A., Piszczek, G., Curth, U., Brautigam, C.A., and Schuck, P. (2014). Measurement of the temperature of the resting rotor in analytical ultracentrifugation. Anal Biochem *458*, 37-39.

Goldenberg, S.J., Cascio, T.C., Shumway, S.D., Garbutt, K.C., Liu, J., Xiong, Y., and Zheng, N. (2004). Structure of the Cand1-Cul1-Roc1 complex reveals regulatory mechanisms for the assembly of the multisubunit cullin-dependent ubiquitin ligases. Cell *119*, 517-528.

Guntert, P., Mumenthaler, C., and Wuthrich, K. (1997). Torsion angle dynamics for NMR structure calculation with the new program DYANA. Journal of molecular biology *273*, 283-298.

Kastner, B., Fischer, N., Golas, M.M., Sander, B., Dube, P., Boehringer, D., Hartmuth, K., Deckert, J., Hauer, F., Wolf, E.*, et al.* (2008). GraFix: sample preparation for single-particle electron cryomicroscopy. Nat Methods *5*, 53-55.

Keller, R.L.J. (2004). Computer Aided Resonance Assignment Tutorial. http://cara.nmr-software.org/downloads/3-85600-112-3.pdf.

Pettersen, E.F., Goddard, T.D., Huang, C.C., Couch, G.S., Greenblatt, D.M., Meng, E.C., and Ferrin, T.E. (2004). UCSF Chimera--a visualization system for exploratory research and analysis. J Comput Chem *25*, 1605-1612.

Pickart, C.M., and Raasi, S. (2005). Controlled synthesis of polyubiquitin chains. Methods in enzymology *399*, 21-36.

Plechanovova, A., Jaffray, E.G., Tatham, M.H., Naismith, J.H., and Hay, R.T. (2012). Structure of a RING E3 ligase and ubiquitin-loaded E2 primed for catalysis. Nature *489*, 115-120.

Sako, K., Suzuki, K., Isoda, M., Yoshikai, S., Senoo, C., Nakajo, N., Ohe, M., and Sagata, N. (2014). Emi2 mediates meiotic MII arrest by competitively inhibiting the binding of Ube2S to the APC/C. Nature communications *5*, 3667.

Sander, B., Golas, M.M., and Stark, H. (2003). Corrim-based alignment for improved speed in single-particle image processing. Journal of structural biology *143*, 219-228.

Sheldrick, G.M. (2008). A short history of SHELX. Acta Crystallogr A *64*, 112-122.

Shen, Y., Delaglio, F., Cornilescu, G., and Bax, A. (2009). TALOS+: a hybrid method for predicting protein backbone torsion angles from NMR chemical shifts. Journal of biomolecular NMR *44*, 213-223.

Sheng, Y., Hong, J.H., Doherty, R., Srikumar, T., Shloush, J., Avvakumov, G.V., Walker, J.R., Xue, S., Neculai, D., Wan, J.W.*, et al.* (2012). A human ubiquitin conjugating enzyme (E2)-HECT E3 ligase structure-function screen. Mol Cell Proteomics *11*, 329-341.

Uzunova, K., Dye, B.T., Schutz, H., Ladurner, R., Petzold, G., Toyoda, Y., Jarvis, M.A., Brown, N.G., Poser, I., Novatchkova, M.*, et al.* (2012). APC15 mediates CDC20 autoubiquitylation by APC/C(MCC) and disassembly of the mitotic checkpoint complex. Nature structural & molecular biology *19*, 1116-1123.

van Heel, M. (1984). Multivariate statistical classification of noisy images (randomly oriented biological macromolecules). Ultramicroscopy *13*, 165–183.

Wickliffe, K.E., Lorenz, S., Wemmer, D.E., Kuriyan, J., and Rape, M. (2011). The mechanism of linkage-specific ubiquitin chain elongation by a single-subunit E2. Cell *144*, 769-781.

Williams, C., van den Berg, M., Panjikar, S., Stanley, W.A., Distel, B., and Wilmanns, M. (2012). Insights into ubiquitin-conjugating enzyme/ co-activator interactions from the structure of the Pex4p:Pex22p complex. The EMBO journal *31*, 391-402.

Wong, L.E., Masse, J.E., Jaravine, V., Orekhov, V., and Pervushin, K. (2008). Automatic assignment of protein backbone resonances by direct spectrum inspection in targeted acquisition of NMR data. J Biomol NMR *42*, 77-86.

Young, T.S., Ahmad, I., Yin, J.A., and Schultz, P.G. (2010). An enhanced system for unnatural amino acid mutagenesis in E. coli. Journal of molecular biology *395*, 361-374.

Zhao, H., Brautigam, C.A., Ghirlando, R., and Schuck, P. (2013a). Overview of current methods in sedimentation velocity and sedimentation equilibrium analytical ultracentrifugation. Current protocols in protein science / editorial board, John E Coligan [et al] *Chapter 20*, Unit20 12.

Zhao, H., Ghirlando, R., Piszczek, G., Curth, U., Brautigam, C.A., and Schuck, P. (2013b). Recorded scan times can limit the accuracy of sedimentation coefficients in analytical ultracentrifugation. Anal Biochem *437*, 104-108.